

**DYNAMIC INTERPLAY BETWEEN CLEAVAGE
FURROW PROTEINS IN CELLULAR
MECHANORESPONSIVENESS**

by
Vasudha Srivastava

A dissertation submitted to Johns Hopkins University in conformity with the
requirements for the degree of Doctor of Philosophy

Baltimore, Maryland

March, 2015

© 2015 Vasudha Srivastava
All Rights Reserved

Abstract

Cell shape changes associated with processes like cytokinesis and motility proceed on several second time-scales. However, they are derived from much faster molecular events, including protein-protein interactions, filament assembly, and force generation. How these molecular dynamics define cellular outcomes remain unknown. While accumulation of cytoskeletal elements during shape change is often driven by signaling pathways, mechanical stresses also direct proteins. A myosin II-based mechanosensory system controls cellular contractility and shape during cytokinesis and under applied stress. In *Dictyostelium*, this system tunes myosin II accumulation under mechanical stress by feedback through the actin network, particularly through the crosslinker cortexillin I. Cortexillin-binding IQGAP proteins are major regulators of this system. We examined the dynamic interplay between these key cytoskeletal proteins using fluorescence recovery after photobleaching (FRAP) and fluorescence correlation spectroscopy (FCS), defining the short time-scale dynamics of these players during cytokinesis and under mechanical stress. Actin and its polar cortex-enriched crosslinkers showed sub-second recovery, while equatorially enriched proteins including cortexillin I, IQGAP2, and myosin II recovered in 1-5 seconds. Mobility of these equatorial proteins was greatly reduced at the furrow, compared to their interphase dynamics. This mobility shift did not arise from a single biochemical event, but rather from global inhibition of protein dynamics by mechanical stress-associated changes in cytoskeletal structure. Thus, the equatorial proteins are stabilized under mechanical stress, which likely enables them to generate contractility at the furrow. We further expanded our genetic and biochemical understanding of this mechanosensory system using a proteomics approach

to identify relevant protein-protein interactions. We identified that, in addition to binding to each other, both cortexillin I and IQGAP2 also interact with myosin II under conditions that prevent myosin II-F-actin binding. Thus, cooperativity between various mechanosensitive elements through macromolecular assemblies may provide a new mechanism for regulating cellular contractility. Mechanical tuning of contractile protein dynamics provides robustness to the cytoskeletal framework responsible for regulating cell shape and contributes to the fidelity of cytokinesis.

Advisor: Douglas N. Robinson, Ph. D.

Reader 1: Marc Ostermeier, Ph. D.

Reader 2: Scot Kuo, Ph. D.

Acknowledgements

This work could not be completed without the constant support and guidance of my advisor, Dr. Douglas N. Robinson. He has been instrumental in the development of this body of work, and my growth as a scientist. I thank him for the freedom given to me to think about the projects, design and interpret experiments and pursue my goals. He has been extremely supportive of me and my career throughout graduate school, and has advised me on all scientific and professional aspects. He has given me numerous opportunities to collaborate on projects, present at conferences, and mentor students. I especially appreciate his help with all the data analysis that allowed me to be productive during a personally challenging time. I want to thank the Department of Chemical & Biomolecular Engineering at the Johns Hopkins University for selecting me for their doctoral program, and for providing a fulfilling graduate experience.

I want to thank all current and past members of the Robinson Lab, especially Cathryn Kabacoff, Sheil Kee, Dr. Corrine Kliment, Dr. Tianzhi Luo, Yixin Ren, Eric Schiffhauer, Dr. Alexandra Surcel, Hoku West-Foyle and Brian Woolums. They have been a great group of colleagues which made every work day enjoyable. Interactions with all of them have had a major impact on my personality and scientific outlook, and I will cherish these relationships throughout my life.

I want to thank my thesis committee members, Dr. Marc Ostermeier and Dr. Denis Wirtz, for their helpful discussions during the committee meetings. I am also thankful to Dr. Scot Kuo, Dr. Erin Goley, Dr. Takanari Inoue and Dr. Zachary Gagnon for being a part

of my GBO committee. I want to thank Dr. Kuo for the numerous discussions about FCS and FRAP, which have helped me think more deeply about the experiments. I would like to thank Dr. Peter Deverotes, Dr. Pablo Iglesias, Dr. Miho Iijima, and their lab groups for the discussions during joint group meetings. I also want to thank Dr. Robert Anders and Dr. Ramana Sidhaye for their inputs during lab meetings. I am extremely thankful to all the staff for Department of Chemical & Biomolecular Engineering, Department of Cell Biology and the JHU-SOM Microscope Facility.

I also thank Dr. Robinson and Ms. Kabacoff for integrating me into the Summer Academic Research Experience. It has been a huge part of my personal and professional growth over the last five years. I thank all the students who have participated in the program for reinforcing my passion for teaching. I would also like to thank all students I have mentored in the Robinson Lab for their help, especially Nurefsan Aksel, Shantel Angstadt, Dina Dajani, and Samantha Miller.

I am grateful to my family for being the constant source of love and support throughout my life. I am grateful to my grandfathers, Late Mr. S.K.Srivastava and Late Dr. J.P.Verma, for being my role models and instilling scientific curiosity in me. I thank my grandmothers, Ms. Prabha Srivastava and Ms. Rekha Verma, for showering me with their love. I am extremely thankful to my parents, Dr. Shakuntala and Dr. Sharad Srivastava, for everything they have done for me. I owe all my accomplishments to their hard work, love and encouragement. I am also very thankful to my uncle, Mr. Shishir Srivastava, and aunt, Ms. Shalini Srivastava, for being second parents to me. I thank my brother

Shashank and my cousins Megha, Sameer, Shobhit, Sadhika and Shreshtha for all the love and memorable times. I also thank my in-laws Ms. Queen Ahuja and Mr. Madan Ahuja for their affection.

I want to thank all my friends for being an integral part of my life. I especially want to thank Krithika Rangarajan, Anshul Rana, Vidya Bhat, Sucheta Arora, Saumya Jain, Mudita Kundra, Pankhuri Vyas, Vidya Sukumar, Aastha Jain, Aditi Swarup, Ambhi Ganesan, Kinshuk Varshney, John Debes, Kirsten Meyer, Emily Newman and Julia Swavola. Finally, I want to thank my husband, Mayank Ahuja, for his companionship through all the good and bad times, for his faith in my abilities, and for constantly pushing me to fulfill my ambitions.

This work was funded by NIH grant GM66817 (to Dr. Robinson), NIH grant S10 OD016374 (to the JHU Microscope Facility), and the Johns Hopkins Physical Sciences in Oncology Center. I am extremely grateful to Isaac Morris Hay and Lucille Elizabeth Hay Graduate Fellowship for funding me for one year.

Table of Contents

Abstract	ii
Acknowledgements	iv
List of Tables	ix
List of Figures	x
1. Introduction	1
1.1 Important players in cytokinesis: A partial parts list	2
1.2 Mechanics of cytokinesis.....	5
1.3 Feedback regulation of cytokinesis and mechanosensing	7
2. Materials and Methods	11
2.1 Cell strains and culture.....	11
2.2 Compression by agarose overlay	12
2.3 Latrunculin-A and jasplakinolide treatment	13
2.4 Fluorescence recovery after photobleaching	14
2.5 Fluorescence correlation spectroscopy	15
2.6 Calculation of diffusion coefficients.....	17
2.7 F-actin quantification by phalloidin and anti-actin staining	18
2.8 Cortical tension measurement using micropipette aspiration	19
2.9 Anti-FLAG coimmunoprecipitation	20
2.10 Mass spectrometric analysis	21
2.11 Tandem Mass Spectrometric Analysis (LTQ-Orbitrap XL).....	22
2.12 Peptide Identification via MASCOT Database Search.....	23

2.13 Comparative analysis of binding partners.....	24
3. Results and Discussion	25
3.1 Equatorial proteins have slower recovery times than polar crosslinkers and exhibit reduced mobility at the cleavage furrow	26
3.2 Genetic control of protein dynamics is suppressed at the furrow	30
3.3 Mechanical stress drives the reduction in cleavage furrow mobility of cortexillin I and IQGAP2.....	36
3.4 Alterations to cortical structure and mechanics shift mobility of cortexillin I.....	41
3.5 Proteomic analysis reveals interactions between myosin II, cortexillin I and IQGAP2.....	46
4. Conclusions.....	50
5. Future Directions	52
5.1 Biochemical basis of mechanosensing.....	52
5.1.1. <i>In vivo</i> characterization of protein-protein interactions	52
5.1.2. <i>In vitro</i> characterization of the myosin II, cortexillin I and IQGAP interactions	53
5.2. Reconstitution of contractile networks to determine the effect of mechanical stress on protein function and dynamics.....	54
5.3. Mechanosensing regulation in dividing mammalian cells.....	56
Appendix.....	58
Contributions.....	69
Bibliography	70
Curriculum Vitae	75

List of Tables

Table 1. Cell strains used in this study	58
Table 2. Mean recovery times and mean immobile fractions for proteins in interphase cells, at the cleavage furrow and in compressed cells	60
Table 3. Mean recovery times and mean immobile fractions for proteins latrunculin-A or jasplakinolide treated cells	61
Table 4. Cytosolic diffusion times (τ_D) and diffusion coefficients (D_{eff}) for proteins as measured by FCS	62
Table 5. Potential cortexillin I-binding proteins	63
Table 6. Potential IQGAP2-binding proteins.....	65
Table 7. Potential IQGAP2-binding proteins in <i>ctxA/B</i> cells	66
Table 8. Potential RacE-binding proteins	67

List of Figures

Figure 1.1	Stages of cytokinesis.....	1
Figure 1.2	Pathways regulating cell mechanics and contractility during cytokinesis .	10
Figure 2.1	Plasmid map for FLAG-GFP-pDM181	12
Figure 2.2	Myosin II accumulates along lateral edges upon compression.....	13
Figure 2.3	Calculation of immobile fraction and recovery time from FRAP	15
Figure 2.4	Calibration of FCS experiments.....	17
Figure 3.1	Cytoskeletal protein dynamics measured by FRAP.....	27
Figure 3.2	Changes in cytoskeletal protein dynamics during cytokinesis	29
Figure 3.3	Cortexillin I and IQGAP2 dynamics at the cleavage furrow	30
Figure 3.4	Changes in cortexillin I and IQGAP2 dynamics at the cleavage furrow in genetic mutants	32
Figure 3.5	Effect of myosin II motor activity on cortexillin I and IQGAP2 dynamics	33
Figure 3.6	Actin dynamics are unchanged in different genetic mutants	33
Figure 3.7	IQGAP2 affects cortexillin I dynamics.....	34
Figure 3.8	Diffusion times for cortexillin I and IQGAP2 measured by FCS.....	35
Figure 3.9	Schematic showing the effect of key cytoskeletal proteins on the dynamics of cortexillin I and IQGAP2, based on FRAP measurements	36
Figure 3.10	Changes in cortexillin I and IQGAP2 dynamics upon compression	38

Figure 3.11	Changes in cortexillin I and IQGAP2 dynamics upon compression in genetic mutants	38
Figure 3.12	Schematic showing the effect of key cytoskeletal proteins on the dynamics of cortexillin I and IQGAP2 under compression	39
Figure 3.13	Protein diffusion upon compression	39
Figure 3.14	The effect of RacE on cortexillin I and IQGAP2 dynamicsx	40
Figure 3.15	GFP dynamics under compression.....	41
Figure 3.16	Perturbation of actin cytoskeleton by latrunculin-A and jasplakinolide....	42
Figure 3.17	Effect of latrunculin-A and jasplakinolide on cell mechanics	43
Figure 3.18	Effect of latrunculin-A and jasplakinolide on protein dynamics	44
Figure 3.19	Effect of latrunculin-A on cortexillin I dynamics in dividing cells	45
Figure 3.20	A schematic showing the changes in protein mobility arise from cytoskeletal rearrangement under mechanical stress or upon latrunculin-A treatment	46
Figure 3.21	Domain organization of cortexillin I and IQGAP1/2	48
Figure 3.22	Selected potential proteins interacting with cortexillin I or IQGAP2, identified by proteomic analysis	49
Figure 5.1	Device for imaging actin networks under stretch	55
Figure 5.2	Myosin II accumulates upon micropipette aspiration in HeLa cells.....	56
Figure 5.3	Myosin IIB is less responsive in anaphase HeLa cells	57

1. INTRODUCTION

Regulation of cell division is critical for normal development as well as disease. An important step in such regulation is ensuring proper cytokinesis, which is the physical separation of a dividing cell into two daughter cells. Cytokinesis proceeds through a series of stereotypical cell shape changes where the cell first rounds up, then elongates forming a cleavage furrow near the middle, whose constriction finally results in the separation of the daughter cells (Fig. 1.1). Cytokinesis failure results in tetraploidy, which leads to aneuploidy and can cause cancer. In contrast, uncontrolled cell division will cause improper partitioning of genetic and cellular material, resulting in cell death. Thus, a detailed analysis of the molecular mechanisms of cytokinesis and their regulation is essential for understanding cellular outcomes and for development of new therapeutic strategies for diseases such as cancer.

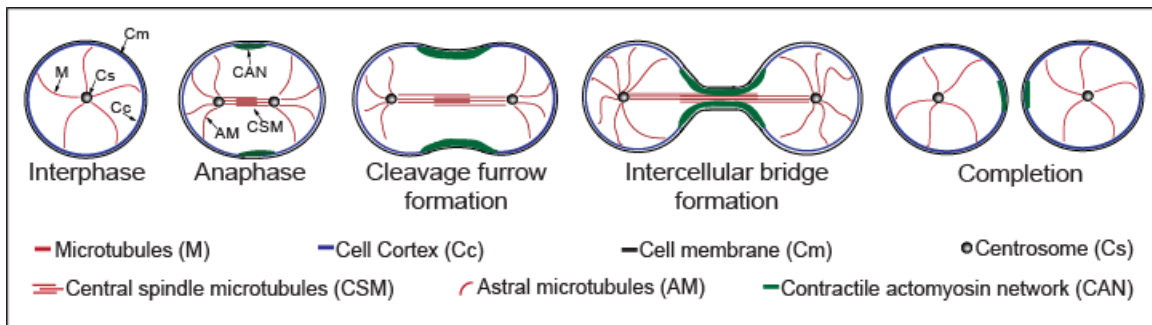


Figure 1.1: Stages of cytokinesis – A schematic diagram depicting the progression of cytokinesis in an amoeboid cell. As the cell elongates during anaphase, a cleavage furrow forms where the contractile actomyosin network is recruited. The furrow continues to ingress to form an intercellular bridge that subsequently separates to form two daughter cells.

The father of modern cytokinesis research, Ray Rappaport said “*When I began working on cytokinesis, I thought I was tinkering with a beautifully made Swiss watch, but what I was really working on was an old Maine fishing boat engine: overbuilt, inefficient, never-failed, and repaired by simple measures.*” [1]. This statement highlights the complexity and built-in redundancy of cytokinesis, which involves crosstalk between several biochemical and mechanical pathways [2-4]. The interplay between these pathways confers the cell with the ability to robustly divide in diverse conditions. The actin cytoskeleton and its associated proteins provide the framework for cytokinesis. The mechanoenzyme myosin II generates contractile force, which causes the cell to constrict in the equatorial region. Different actin crosslinkers and anchoring proteins play structural roles and help propagate forces within the actin network. The spatiotemporal localization of these proteins at the cell cortex during cell division is critical to ensure successful cytokinesis.

1.1.Important players in cytokinesis: A partial parts list

In most eukaryotic cell types, actin and the motor protein myosin II are known to form a contractile structure in the equatorial region of a dividing cell, whose ingression drives cytokinesis. Actin controls the cell mechanics by forming a highly dynamic network of semi-flexible filaments. During the myosin II power stroke, myosin II pulls on the actin filaments as it releases the ATP hydrolysis products, thereby generating mechanical force. Two myosin II heavy chains combine with two essential and two regulatory light chains (ELC and RLC respectively) to form a myosin II hexameric monomer. Two monomers combine to form a parallel myosin II dimer, which then assembles into

functional bipolar thick filaments (BTFs) by dimer addition [5, 6]. Rho-kinase (ROCK) directs BTF assembly by activating myosin II through the phosphorylation of RLC. Additionally, heavy chain phosphorylation also controls BTF assembly and disassembly, both of which are required for normal cytokinesis [7]. Though myosin II is the major mechanoenzyme during cytokinesis, it is not necessary for cytokinesis. Adherent *Dictyostelium* cells can divide fairly normally in the absence of myosin II using traction forces to help with the initial cell elongation followed by cortical tension-driven furrow thinning [8, 9]. The effects of cortical tension, which serves to minimize the surface area-to-volume ratio, are highly reminiscent of the surface tension of a liquid droplet, which also helps drive droplet breakup.

In addition, several other actin-binding proteins, such as anillin and α -actinin in mammals and cortexillin I in *Dictyostelium*, help form a cross-linked actin network in the cell cortex and regulate the mechanical properties of the cortex during cytokinesis [10, 11]. These proteins differ in their structure, actin-binding kinetics, force sensitivity and cellular localization. The actin crosslinkers and myosin II collectively bear the force in the cortex. Some crosslinkers also contain lipid-binding domains (such as the pleckstrin-homology (PH) domain) that facilitate membrane attachment of the actin meshwork. In animal cells, anillin is a potential scaffolding protein that may provide membrane anchoring and link Rho, actin and myosin II in the furrow [10]. Rho is a major regulator of animal cytokinesis, as it controls both actin polymerization through formins and myosin II activation through ROCK [12, 13]. The levels of GTP-bound active Rho in the

cleavage furrow are controlled by the guanine-exchange factor (GEF) ECT2 and the GTPase-activating protein (GAP) MgcRacGAP [14].

The microtubules and its associated proteins are also important for spatiotemporal regulation of cytokinesis. In most cells, cytokinesis occurs in the plane perpendicular to the mitotic spindle near the center of the cell. Thus, the spindle can deliver signals to the cell cortex that modulate cortical mechanics and direct cleavage-site selection and actomyosin contractile structure formation. This signal can either be in the form of a biochemical factor or a purely mechanical cue like a change in cortical tension or membrane potential. Many microtubule-based proteins such as the kinesin-6 family of proteins (mitotic kinesin-like protein-1, MKLP-1) are known to be important in cytokinesis and may localize asymmetrically in a dividing cell [14]. These proteins are believed to promote communication between the central spindle and the cell cortex. The astral microtubules, which point away from the spindle, are also important for regulating mechanics and inhibiting contractility in the polar cortex [15, 16].

Even though the plasma membrane is thought to have a relatively limited contribution to the cellular mechanical properties, proteins involved in membrane dynamics, membrane fission and fusion, and vesicle transport are important in cytokinesis. The surface area of a dividing cell increases significantly as the furrow constricts [3, 17]. This requires the deposition of new membrane in the furrow region. In addition, constant membrane remodeling is required to relieve mechanical stress. Also, the plasma membrane is an important scaffold for many signaling proteins. As the search for new genes that regulate

cytokinesis continues, many non-protein factors, including lipids and small metabolites, are also being examined as regulators of cytokinesis. For example, the phosphoinositol-4,5-bisphosphate (PIP2) is enriched in the cleavage furrow and can control the accumulation and retention of PIP2-binding proteins during cytokinesis [18, 19]. In addition, many mechanical parameters, such as those described in the mechanics of cytokinesis section, can affect the kinetics of cell division. To ensure robustness of cytokinesis, current models support the existence of multiple interacting, as well as parallel, mechanisms, thereby making the compilation of a comprehensive cytokinesis parts list challenging.

1.2.Mechanics of cytokinesis

Cytokinesis is fundamentally a mechanical process that requires major reorganization of the actin cytoskeleton and its associated proteins to promote cellular contractility at the cleavage site. Hence, it is essential to supplement biochemical and genetic information with biophysical and mechanical studies to understand force generation, sensing, and transduction in a dividing cell. A diverse tool set is available to study cell mechanics during cytokinesis, allowing characterization of various mechanical parameters [20]. While micropipette aspiration (MPA) studies are used to determine the elastic modulus and effective cortical tension, atomic force microscopy (AFM) measures the bending modulus. The elastic modulus determines the deformability of the cell surface, and the cortical tension is a complex parameter that measures the energy cost per unit increase in cell surface area [3]. The bending modulus reflects the stress required for bending a material. During cytokinesis, the initial deformation of a roughly spherical cell requires

deviation from its quasi-steady state. This is resisted by the cortical surface tension, which favors a spherical cell. However, as the furrow continues to ingress, the curvature in the cleavage furrow changes so that the cortical tension actually favors bridge thinning and abscission [3, 21]. Laser tracking microrheology (LTM) can be used to measure cortical viscoelasticity non-invasively. Viscoelasticity represents the time-dependent cellular response to stresses and affects the kinetics of furrow ingression by dampening the mechanical deformation, thereby allowing sufficient time for activation and stabilization of biochemical factors [3, 21].

Disruption of actin filaments by compounds such as latrunculin-A has established that the actin cytoskeleton is the main contributor of cell mechanics, though the cell membrane and microtubules also make some contribution [16, 22]. The actin cytoskeleton also undergoes remodeling with internally or externally generated mechanical stresses. The impact of these mechanical stresses has been uncovered using micropipette aspiration, which allows the application of a defined, localized stress on the cell, similar in magnitude to stresses experienced during cytokinesis [23]. Many proteins such as myosin II, which localize to the cleavage furrow cortex, also accumulate at sites where mechanical stress has been applied [6, 24, 25].

In addition to the mechanical activation of biochemical reactions, the mechanical properties of the cell can be controlled biochemically. Knockdown or deletion of many actin crosslinkers and associated proteins softens the cell cortex significantly, leading to altered furrow ingression kinetics and a reduced ability to perform cytokinesis in

suspension culture (where cell-substrate adhesion is absent) [6, 25-27]. The biochemical constitution of the cell cortex governs its physical properties and determines how proteins respond to mechanical stresses. For example, in the absence of myosin II, certain crosslinkers such as α -actinin show greater accumulation to sites of applied mechanical stress, while the myosin II mechanosensory response is amplified in mutants depleted of the small GTPase RacE which affects several polar crosslinkers [28]. Structurally, these crosslinkers can be divided based on their actin binding properties as those which form actin bundles and those which promote the formation of a crosslinked meshwork, which drives the sensitivity of their response to mechanical stress and accompanying network deformations [28].

In *Dictyostelium*, the cortex becomes highly mechanoresponsive upon the onset of anaphase, where myosin II and cortexillin I show accumulation at lower pressures [24, 28]. Interestingly, the overall deformability of the furrow is lower than the polar cortex, even though furrow undergoes major deformation during cytokinesis, which is attributed to an asymmetric cortical distribution of mechanosensitive proteins during cytokinesis [27]. This further illustrates the role of biochemical pathways in regulating cell mechanics. These findings demonstrate the intricate interplay between biochemical and mechanical pathways during cytokinesis.

1.3. Feedback regulation of cytokinesis and mechanosensing

As illustrated above, cytokinesis involves several proteins having multiple modes of regulation that controls when and where division occurs. This multi-level regulation can

be emphasized using *Dictyostelium* cytokinesis as an example. The amoeba *Dictyostelium discoideum* is a powerful model for cytokinesis studies due to its genetic homology and mechanical similarity to many mammalian cells, as well as its amenability for genetic, biochemical and mechanical perturbations.

As the cell starts to divide, myosin II is enriched in the equatorial region where the cleavage furrow forms. Cortexillin I, an actin crosslinker, also accumulates at the furrow where it regulates contractility along with myosin II [6]. The cooperative interactions between myosin II and cortexillin I are mechanosensitive and are mediated by actin filaments [5]. Both these proteins are also recruited to sites of applied stress during micropipette aspiration [5, 6]. Thus, these proteins form the core of a mechanoresponsive contractile unit, where myosin II is the force-generating element and cortexillin I anchors the actin network, and helps propagate forces through this network. During cytokinesis, signals from the mitotic spindle direct the symmetry breaking and the initial recruitment of these proteins to the cell equator (**Fig. 1.2**). Subsequently, the mechanical feedback between myosin II and cortexillin I controls the protein amount, and the contractility, at the furrow. Further, two cortexillin I-binding proteins, IQGAP1 and IQGAP2, provide additional regulation of this mechanoresponsive system [25] (**Fig. 1.2**). In the absence of IQGAP2, myosin II and cortexillin I fail to accumulate in response to applied stress due to inhibition by IQGAP1. However, double mutant lacking both IQGAPs is highly mechanoresponsive indicating the IQGAPs are not required for mechanoresponsiveness, and only play regulatory roles. Further, IQGAP2 also transduces the readout from the mechanosensor back to the spindle signaling proteins. It is required for directing stress-

dependent accumulation of the mitotic kinesin-like protein (MKLP) Kif12 and the chromosome passenger complex protein INCENP to the cell cortex upon aspiration [25] (**Fig. 1.2**).

In addition to regulation at the cleavage furrow, the global cell mechanics are also highly controlled during cytokinesis. Many actin crosslinkers such as dynacortin and fimbrin are enriched in polar cortex, and contribute to cortical dynamics [26, 27]. The small GTPase RacE is a global regulator of cortical mechanics and cytokinesis [29], and acts upstream of many actin crosslinkers including dynacortin and coronin [3, 21, 30] (**Fig. 1.2**). The overexpression of polar crosslinker inhibits myosin II mechanoresponsiveness, while the absence of RacE or dynacortin makes myosin II more responsive. During cytokinesis, the equatorial mechanoresponsive unit (comprising of myosin II and cortexillin I) and the polar module (comprising RacE and other actin crosslinkers) exhibit inverse concentration gradient, promoting furrow ingression. Though the equatorial and polar modules have complementary roles during cytokinesis, there is crosstalk between these modules. RacE also acts upstream of 14-3-3, which is enriched in the polar cortex where it regulates cortical tension and steady state microtubule length [16] (**Fig. 1.2**). 14-3-3 also binds to the myosin II heavy chain and promotes myosin II bipolar thick filament turnover at the furrow [16]. Thus, myosin II contractility at the furrow is regulated by the interplay between the equatorial regulatory module and the polar cortex proteins [4].

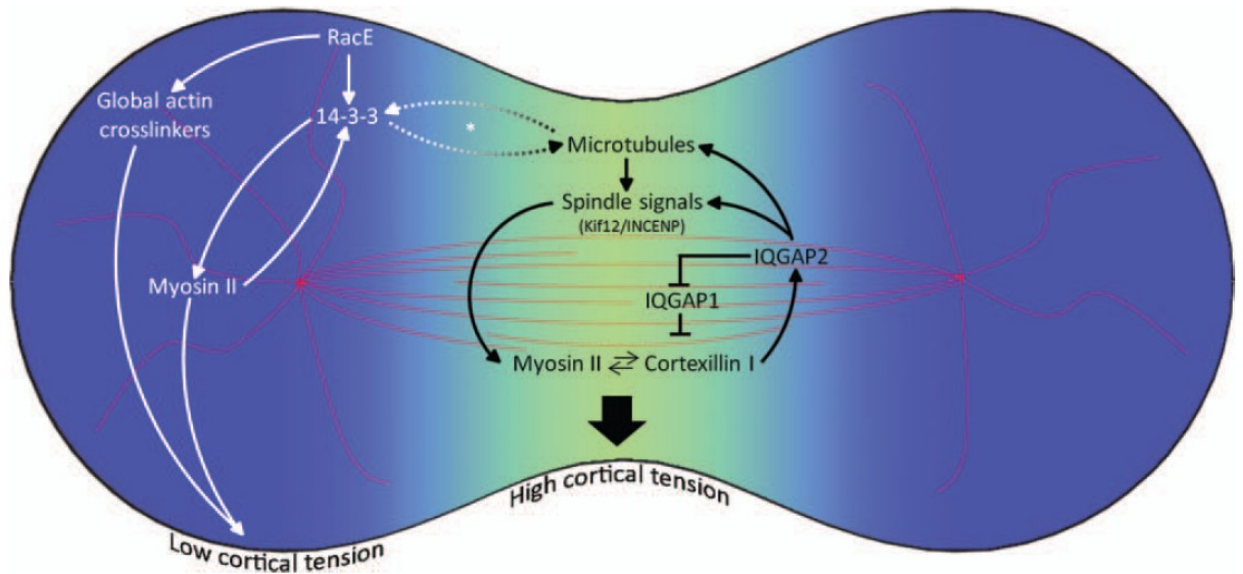


Figure 1.2: Pathways regulate cell mechanics and contractility during cytokinesis. An equatorial module, comprising of myosin II, cortexillin I, IQGAPs and kif12/INCENP, tunes myosin II recruitment at the furrow. The RacE-14-3-3-myosin II pathway and the polar crosslinkers control cortical tension at the poles. The signals from the mitotic spindle as well as the astral microtubules are central in directing the spatiotemporal function of these modules during cytokinesis [4].

Though the roles of myosin II and many actin crosslinkers in cytokinesis and contractility have been examined carefully, the molecular mechanisms for the recruitment and retention of these proteins remain unknown. For example, a myosin II mutant lacking the motor domain can be enriched to the furrow region, though it is not tightly incorporated in the cortex suggesting that additional pathways may regulate myosin II furrow recruitment [31]. A genetic selection has identified novel roles for many proteins, including RMD1 (regulator of microtubule dynamics-1) and mmsdh (methylmalonate semialdehyde dehydrogenase), in rescuing defects in myosin II BTF assembly and furrow enrichment [32]. Thus, multiple parallel pathways regulate myosin II furrow localization and cellular contractility, thereby providing robustness to the cellular cytokinesis machinery. Hence, Rappaport appropriately concluded that cytokinesis is indeed a complex shape change process, which is over-built and is hard to fail.

2. MATERIALS AND METHODS

2.1. Cell strains and Culture

A complete list of the strains used is provided in **Table 1**. Cells were grown in Hans' enriched 1.5X HL-5 media (enriched with 8% FM medium) containing penicillin and streptomycin at 22⁰C on polystyrene petri dishes. Wild type strains used were KAx3 [33], Ax3:Rep orf+ (HS1000) [30] and rescued strains. Mutant cell lines used have been described previously – *myoII* [33], *ctxA*, *ctxB*, and *ctxA/B* [30, 34], *iqg1*, *iqg2* and *iqg1/2* [34], and *racE* [30]. The plasmids for RFP-tubulin, GFP-cortexillin-I, GFP-IQGAP2, GFP-actin, mCherry-myosin-II and GFP have been described previously [24, 25, 28, 34]. Cells were transformed with expression plasmids by electroporation using a Genepulser-II electroporator (Bio-Rad, Hercules, CA).

For the coimmunoprecipitation studies, FLAG-GFP-tagged constructs were made for cortexillin I, IQGAP2 and RacE by cloning into the pDM181 vector. The FLAG-GFP plasmid was used as a negative control. A FLAG-GFP DNA fragment was amplified by polymerase chain reaction using the following primers:

5'BglII-RBS-FLAG-SacI-GFP (Forward primer):

5' AAA AAA AGA TCT CTA TTA AAA TGG ATT ATA AAG ATG ATG ACG ATA AAG AGC TCA TGG ATC CAT CGA AAG GTG AAG 3'

3'SalI-Linker-SacI-GFP (Reverse primer):

5' AAA AAA GTC GAC GGA TCT TGA TAT CTT ACC TGA ACC TGA ACC GAG CTC TTT GTA TAG TTC ATC CAT GCC ATG TG 3'

The amplified DNA was then cloned into pDM181 vector using BglII and SalI restriction enzymes. Subsequently, cortexillin I, IQGAP2 or RacE were cloned into this plasmid using SalI and NotI sites in the vector. The plasmid map for FLAG-GFP-pDM181 is given below.

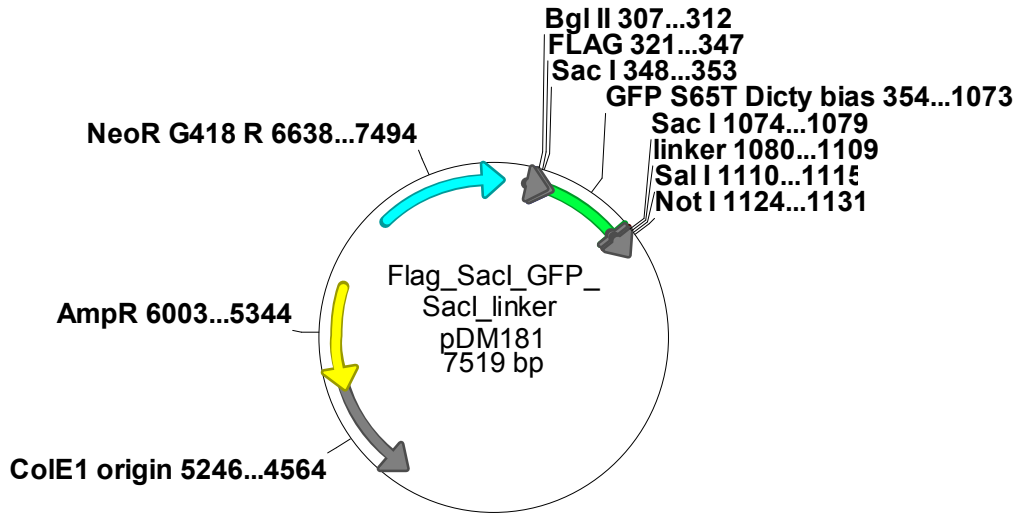


Figure 2.1: Plasmid map for FLAG-GFP-pDM181.

Cells were then grown in selection medium containing 15 $\mu\text{g}/\text{mL}$ G418 or 40 $\mu\text{g}/\text{mL}$ hygromycin or both drugs when transforming two plasmids. Expression levels were checked by fluorescence imaging or Western blotting. Cells with comparable fluorescent protein expression were used for the experiments.

2.2.Compression by Agarose Overlay

Agarose overlay has been established as a method for applying uniform global mechanical stress, and has previously been shown to drive mechanosensitive accumulation of certain proteins at the cell cortex [25] (Fig. 2.2). For compression, thin sheets of 2% agarose in MES starvation buffer (50 mM MES pH 6.8, 2 mM MgCl_2 and

0.2 mM CaCl₂) were prepared according to the protocol described by Fukui *et al.* [35, 36] and modified by Kee *et al.* [25]. The cells were plated in imaging chambers for 1 hour. The culture medium was aspirated and cells were washed with MES starvation buffer twice to reduce the background fluorescence. The buffer was removed completely and a sheet of agarose was carefully placed to cover the cells. Imaging was started after the cells were completely flattened (about 2 minutes). To ensure proper cell health, the flattened cells were not used beyond 10 minutes and were replaced during experiments.

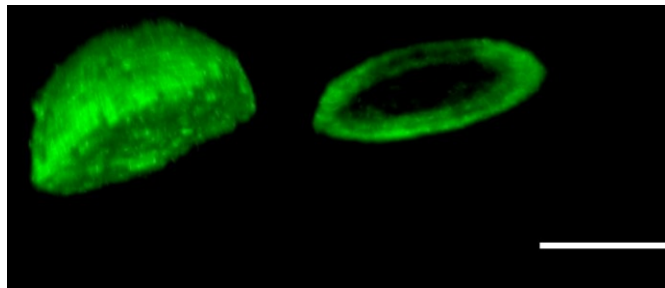


Figure 2.2: Myosin II accumulates along the lateral edges upon compression in regions of maximum stress. 3D-reconstruction of GFP-myosin II expressing *Dictyostelium* cells in absence or presence of compression.

2.3. Latrunculin-A and Jasplakinolide Treatment

Latrunculin-A and Jasplakinolide were obtained from Sigma-Aldrich. All cells were pre-treated with 0.1% DMSO for 4-6 hours. For phalloidin and anti-actin staining, the cells were incubated with the drugs for 15 minutes. For live cell imaging, drug stocks were freshly made in MES starvation buffer. The cells plated in imaging chambers were washed with MES starvation buffer + 0.1% DMSO, followed by the addition of the drug-containing buffer. Imaging was performed after a 10 minute incubation, and each slide was imaged for 15 minutes before it was replaced with a new slide.

2.4. Fluorescence Recovery after Photobleaching (FRAP)

FRAP experiments were performed using a Zeiss Axiovert 200 inverted microscope with LSM510-Meta confocal module, with a 63x (NA 1.4) objective. Cells expressing GFP-tagged proteins were plated in glass-bottom imaging chambers for an hour. The culture medium was replaced with MES starvation buffer immediately before imaging. A small region of the cell cortex was bleached using a 488 nm Argon laser, and the fluorescence recovery was recorded until recovery saturated (150 frames, 45-150 ms/frame depending on the protein). The size and placement of the bleach region was kept relatively constant across measurements.

For each frame, the average intensity of the bleached cortical region, reference (unbleached) region, and background was quantified using ImageJ (National Institutes of Health, Bethesda, MD) (**Fig. 2.3A-B**). For photobleaching correction, the reference theoretical intensity (RTI) was calculated by fitting the background subtracted reference intensity to an exponential decay equation as follows:

$$RTI(t) = A - B \cdot e^{-C \cdot t} \quad (1)$$

Where, A, B and C are fitting parameters.

The intensity of the bleached region was background subtracted and normalized to RTI (**Fig. 2.3C**). The normalized intensity (NI) was obtained by normalizing this to the pre-bleach intensity (average of 4 pre-bleach images), and was fitted to a single exponential as follows:

$$NI(t) = m_1(1 - m_2 \cdot e^{-kt}) \quad (2)$$

Where, m_1 , m_2 are fitting parameters and k is the recovery rate.

The recovery time, τ , and the immobile fraction, F_i were measured as:

$$\text{Recovery time, } \tau = 1/k \quad (3)$$

$$\text{Immobile fraction, } F_i = \frac{1-m_1}{1-m_1+m_2} \quad (4)$$

We also plotted the derivative of normalized intensity for each protein to confirm that our data fit a single-exponential, and did not require more complicated models. The recovery times and immobile fractions calculated from FRAP are summarized in **Tables 2-3**.

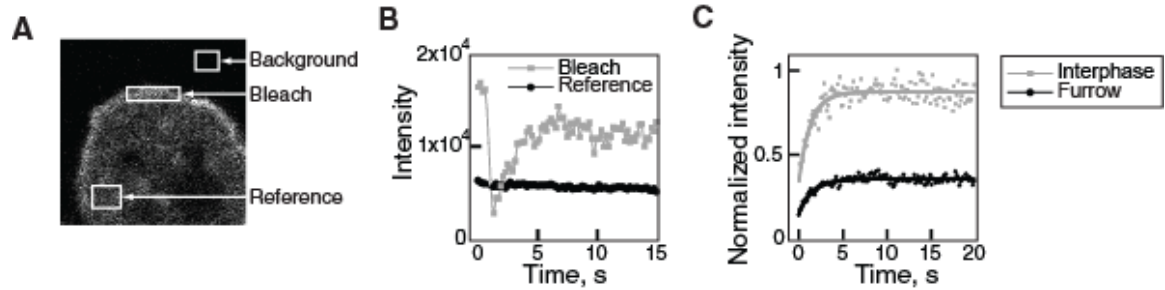


Figure 2.3: Calculation of immobile fraction and recovery time from FRAP. (A) An example confocal image of a GFP-cortexillin I-expressing cell illustrating the bleach, reference and background region used for FRAP measurements. (B) Example fluorescence intensity curves showing changes in intensity of bleached and reference regions during a FRAP experiment. (C) Example traces showing fluorescence recovery of GFP-cortexillin I in interphase and cleavage furrow cortex.

2.5. Fluorescence Correlation Spectroscopy (FCS)

FCS experiments were performed using a Zeiss AxioObserver with 780-Quasar confocal module & FCS, with a C-Apochromat 40x (NA 1.2) water objective. For purified proteins and dyes, the imaging plane was set 200 μm above the coverslip. 10 repetitions of 5 seconds each were collected and the average spectrum was used for measuring diffusion times. For diffusion measurements in cells, the imaging plane was set through

the middle of the cell. The acquisition time was reduced to 2 seconds to avoid complications from long range cellular and intracellular movement. The average from 2-7 repetitions was used to calculate diffusion times. Any trace showing a persistent deviation from the mean or significant photobleaching was discarded. The autocorrelation data was then fit to a single component, 3D-diffusion model with triplet state dynamics using the following equation:

$$g(\tau) = G_{triplet} \cdot \frac{1}{N} \cdot \left(1 + \frac{\tau}{\tau_D}\right)^{-1} \cdot \left(1 + \frac{\tau}{\gamma^2 \tau_D}\right)^{-0.5} \quad (5)$$

Where,

τ = correlation time

τ_D = diffusion time

N = number of particles

γ = structural parameter

$$G_{triplet} = \frac{1 - \theta_T + \theta_T \cdot e^{-\tau/\tau_T}}{\theta_T}$$

(θ_T = fraction of particles in triplet state and τ_T = relaxation time for triplet state).

100 nM Rhodamine 6G was used for pinhole alignment and structural parameter calculation (**Fig. 2.4**). The measured value of the structural parameter was used for diffusion time calculation of other proteins. All imaging was done in uncoated 35 mm-glass bottom dishes (Coverslip No. 1.5) (MatTek Corp., Ashland, MA).

In compressed cells, the cell height is comparable to the z-dimension of the FCS confocal volume. Therefore, we also analyzed the FCS data using a 2D-diffusion model and

observed no significant differences in diffusion times as compared to those calculated using the 3D-diffusion model.

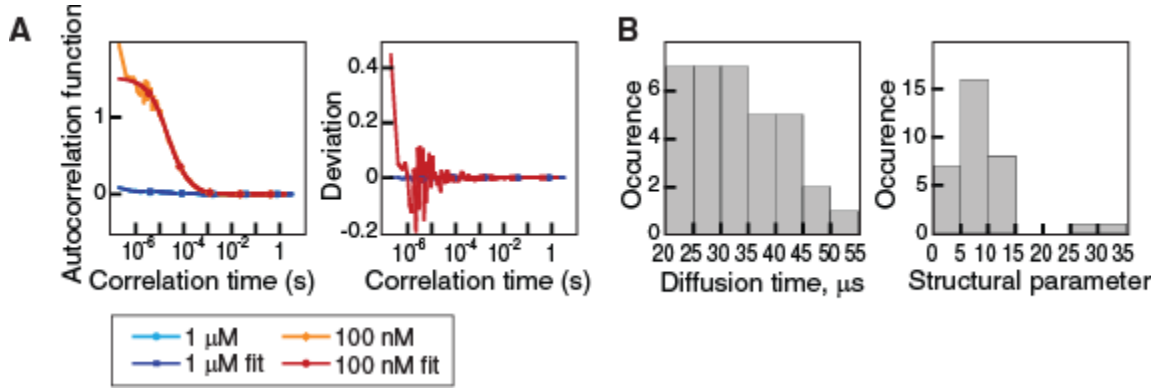


Figure 2.4: Calibration of FCS experiments: (A) Example autocorrelation curves for rhodamine 6G diffusion as measured by FCS. The autocorrelation data was fitted to a 1-component 3D diffusion model with triplet state dynamics. The panel on right is the residual curve showing the goodness of fit. (B) The distribution of diffusion times and structural parameter measured for rhodamine 6G by FCS.

2.6. Calculation of Diffusion Coefficients

Rhodamine 6G was used as a standard for calculating diffusion coefficients. As the diffusion coefficient is inversely proportional to the diffusion time, we used the published value of the diffusion coefficient for rhodamine 6G and measured diffusion times for rhodamine 6G and the proteins of interest to calculate effective diffusion coefficients (D_{eff}).

$$D_{eff} = \frac{D_{R6} \cdot \tau_{D,R6}}{\tau_D} \quad (6)$$

Where,

D_{R6} = diffusion coefficient for rhodamine 6G (= 426 $\mu\text{m}^2/\text{s}$ [37])

$\tau_{D,R6}$ = measured diffusion time for rhodamine 6G = $33 \pm 2 \mu\text{s}$

τ_D = measured diffusion time.

We used purified mCherry to validate our diffusion coefficient calculation. Our measured diffusion coefficient for mCherry ($94 \mu\text{m}^2/\text{s}$) matched closely the published value for purified GFP ($95 \mu\text{m}^2/\text{s}$ [37]) under the same conditions (**Table 4**). All diffusion time measurements and estimated diffusion coefficients are summarized in **Table 4**.

2.7.F-actin Quantification by Phalloidin and Anti-actin Staining

For quantifying the relative amount of F-actin, the cells were fixed and stained with TRITC-phalloidin (Sigma Aldrich) or anti-actin monoclonal antibody (Developmental Studies Hybridoma Bank, University of Iowa) as described in *Luo et al.* [5]. *Dictyostelium* cells were plated on sterile 22x22 mm glass coverslips in 6-well polystyrene dishes at 70-80% confluency for 1 hour. The media was aspirated and replaced with 2 mL drug-containing media for 15 minutes. The cells were washed with 1X PBS, and immediately fixed on ice using acetone at -20°C for 3 minutes. The coverslips were transferred to a new 6-well dish and washed once with 1X PBS, followed by blocking in blocking buffer (1X PBS + 0.05% Triton X-100 + 0.5% BSA) for 30 min. The cells were stained with $0.16 \mu\text{M}$ TRITC-phalloidin for 1 hour or with anti-actin antibody overnight followed by 2 hour incubation with TRITC goat-anti-mouse secondary. All coverslips were washed 4 times with 1X PBT (1X PBS + 0.05% Triton X-100) for 5 minutes each, and then once with 1X PBS. The coverslips were then mounted on glass slides using $10 \mu\text{L}$ mounting buffer (90% glycerol in 1X PBS).

To quantify the relative amount of F-actin, all coverslips were imaged under identical conditions on a motorized Olympus IX71 microscope using a 40x (NA 1.3) objective with a 1.6x optovar (Olympus, Center Valley, PA). The integrated fluorescence intensity of the cells was quantified using ImageJ. At least 100 cells from more than 10 different fields were quantified. The intensity was normalized to the average fluorescence intensity of the untreated control for a given experiment. The data shown represents three biological replicates.

2.8.Cortical Tension Measurement Using Micropipette Aspiration

The experimental set-up has been previously described in detail in Effler *et al.* (2006). 0.01-0.6 nN/ μm^2 pressures were applied to a smooth region of the cell cortex through a $\sim 5 \mu\text{m}$ internal diameter glass micropipette ($R_p = 2.3\text{-}3 \mu\text{m}$). A low pressure was first applied to form a pressure seal. The cell protrusion was allowed to stabilize for 30 seconds before imaging. Subsequently, the pressure was gradually increased and imaging was resumed after the protrusion stabilized. This was continued until the protrusion length became large ($L_p > R_p$) or the cell blebbed. At each pressure, the protrusion length from five consecutive frames was averaged. The critical pressure (ΔP_{crit}) was identified as the pressure where $L_p = R_p$, and the cortical tension (T_{eff}) was calculated using the following equation:

$$\Delta P_{\text{crit}} = 2T_{\text{eff}} \cdot \left(\frac{1}{R_p} - \frac{1}{R_c} \right) \quad (7)$$

2.9. Anti-FLAG Coimmunoprecipitation

The cytoskeletal fractionation protocol was modified from Reines and Clarke [38]. The cells were gently dislodged from the plate and centrifuged at 4000g for 5 minutes. The cells were washed with 1X PBS and resuspended to a final concentration of 5×10^7 cells/mL for the 'cytoskeletal' sample (C) and 1×10^7 cells/mL for the 'soluble' sample (S). The cells were centrifuged at 5000g for 5 minutes, resuspended in 500 μ L Lysis Buffer (100 mM PIPES pH 6.8, 2.5 mM EGTA, 1 mM $MgCl_2$, 1 mM ATP, 0.5% Triton X-100 and protease inhibitor cocktail) and incubated on ice for 10 minutes with intermittent vortexing. The samples were centrifuged at 15000g for 5 minutes at 4⁰C. The supernatant from 'soluble' sample was transferred to a fresh tube and kept on ice for coimmunoprecipitation. The pellet from the 'cytoskeletal' sample was dissolved in Release Buffer (100 mM PIPES pH 6.8, 2.5 mM EGTA, 1 mM $MgCl_2$, 1 mM ATP, 200 mM NaCl and protease inhibitor cocktail), and incubated on a tube rotator for 15 minutes at 4⁰C. The 'cytoskeletal' sample was then centrifuged at 15000g for 5 minutes at 4⁰C, and the supernatant was processed for coimmunoprecipitation.

Forty-microliters IgG-Agarose beads and 40 μ L anti-FLAG M2 Affinity Gel (Sigma Aldrich) per sample were aliquoted and washed three times with 1X TBS (50 mM Tris pH 7.4 and 150 mM NaCl). To reduce non-specific binding, the supernatants from cytoskeletal fractionation were incubated with 40 μ L IgG-Agarose beads for 30 minutes at 4⁰C with continuous mixing. The samples were centrifuged at 5000g for 1 minute, and the supernatants were transferred to tubes containing 40 μ L pre-washed anti-FLAG resin, and incubated overnight at 4⁰C. The resin was washed four times with 1X TBS, and

eluted with 0.1 M glycine, pH 3.5. The eluted samples were then analyzed by mass spectrometry to identify potential binding partners.

2.10. Mass Spectrometric Analysis

Forty-microliters of eluted samples were incubated with 10 mM of tris-2 carboxyethyl phosphine (Sigma) for 20 min at RT with shaking, followed by alkylation with 10 mM of IAA (Sigma) for 20 min, at ambient RT, protected from light. The reduced and alkylated proteins were acetone precipitated to remove solutes not compatible with downstream LC/MS/MS analysis. Final pellet was air-dried. 5 µg of endoproteinase Lys-C (Promega, Madison, WI) was reconstituted in 650 µL of digestion solution (0.1% RapiGest (Waters, Milford, MA), 20% ACN, 50 mM Ammonium Bicarbonate). 20 µL of that solution was added to each acetone precipitated sample. Protein pellet was allowed to digest for 2 hours at 37⁰C with constant shaking. Following addition of 1 µg of trypsin (Promega, Madison, WI) in 20 µL of digestion solution, enzymatic proteolysis continued overnight under the same conditions. TFA was added to deactivate enzymes. Samples were desalted using UltraMicro Spin C18 columns (NestGroup, Southborough, MA) according to the manufacturers instructions. Collected peptides were lyophilized and reconstituted in 10 µL of water with 0.1% fluoroacetic acid (FA) Optima (Thermo Fisher Scientific).

Four-microliter aliquots of each tryptic protein digest solution were analyzed on EASY n-LC 1000 (Thermo Scientific) coupled to Orbitrap-Elite (Thermo Fisher) mass spectrometer. Peptides were separated on Acclaim PepMap RSLC column (Thermo

Scientific), with 50 μm inner diameter, 15 cm length, packed with C18 reversed phase 2 μm particles, 100 Å pore size), using mobile phase linear gradient from 5% B to 20% B in 40 min continued to 35% B in 10 min at 300 $\mu\text{L}/\text{min}$ flow rate, where mobile phase A was composed of 0.1% (v/v) Formic acid in water and mobile phase B 0.1% (v/v) Formic acid in acetonitrile.

2.11. Tandem Mass Spectrometric Analysis (LTQ-Orbitrap XL)

Eluting peptides were ionized via Nanospray Flex ion source (Thermo Scientific) operated at following settings: source voltage 2.00V, capillary temperature 275.00 C and S-lens RF level 60.

The Orbitrap –Elite mass spectrometer was operated in *data dependent* mode. MS precursor scan spectra (m/z 350-1800) were acquired in the Orbitrap with mass resolution of 60,000 full-width half-maximum (at m/z 400). The fifteen most intense ions from each MS scan were automatically targeted for CID (collision induced dissociation) fragmentation (MS/MS) in the LTQ (linear ion trap) with dynamic exclusion 90 sec. For MS1, AGC (automatic gain control) target was set to 1×10^6 with maximum accumulation time 250 ms. Only ions of 1000 minimum signal intensity were selected for MS2 fragmentation. MS2 spectra were acquired in a rapid scan mode in the LTQ (linear ion trap) using targeted setting of 10×10^4 ions and accumulation time of 150 ms. Normalized collision energy was set at 35%. The default charge state was set at two. The isolation window for the ion gate was fixed at two Daltons. The activation Q was set at 0.25.

2.12. Peptide Identification via MASCOT Database Search

Raw MS data were searched against the UniProt *Dictyostelium discoideum* database. (37,261 entries; October, 2013 version) using Sorcerer 2™-SEQUEST® (Sage-N Research, Milpitas, CA) with postsearch analysis performed using the Trans-Proteome Pipeline, implementing PeptideProphet and ProteinProphet algorithms. Sequest (Thermo Fisher Scientific, San Jose, CA: version 1.0) was set up with following search parameters: semienzyme digest using trypsin (after Lys or Arg) with up to two missed cleavages; monoisotopic precursor mass range of 400–4500 amu; and oxidation (Met), carbamidomethylation (Cys), and acetylation(Lys) were specified as variable modifications. Peptide mass tolerance was set to 50 ppm, fragment mass tolerance was set to 1 amu, fragment mass type was set to monoisotopic, and the maximum number of modifications was set to four per peptide.

Scaffold (version Scaffold_4.4.1.1, Proteome Software Inc., Portland, Or) was used to validate peptide and protein identifications. Error rates (false discovery rates) and peptide probabilities (p) were calculated by Peptide Prophet, accepted peptide identifications had greater than 95% probability with Scaffold delta-mass correction. Protein Probabilities were assigned by Protein Prophet algorithm, only proteins identification at greater than 95% probability, which contained at least two identified peptides were reported.

2.13. Comparative analysis of binding partners

The normalized spectral counts were used for identifying proteins that were up- or down-regulated in the experimental samples as compared to the control group based on quantifying the protein total spectral count. We applied the G-test of independence to determine the significance of difference in the normalized spectral count (average of 3 replicates) for the experimental and control group. We defined f_1 = normalized spectral counts/protein in the control sample (FLAG-GFP), f_2 = normalized spectral counts/protein in the experimental sample (FLAG-GFP-cortexillin I, for example). When a protein was absent from one of the samples, it was assigned the normalized spectral count of 0.0001. The G value was calculated as

$$G = 2f_1 \ln\left(\frac{f_1}{avgf_1}\right) + 2f_2 \ln\left(\frac{f_2}{avgf_2}\right)$$

Where $avgf_1 = avgf_2 = (f_1 + f_2)/2$

A Chi-squared distribution with one degree of freedom was assumed, with a p value less than 0.05 considered significant. Thus, a protein was considered differentially expressed if the calculated G value was greater than 3.841.

3. RESULTS AND DISCUSSION

Cytokinesis is a complex shape change process involving a large number of proteins which work together in a highly coordinated manner. The crosstalk between various cytoskeletal modules ensures high fidelity of cytokinesis. Previous genetic and mechanical studies in *Dictyostelium* have identified a mechanoresponsive control system that regulates contractility at the cleavage furrow of a dividing cell. The mitotic spindle and mechanical stress direct recruitment of contractile proteins – myosin II and cortexillin I – at the furrow, driving furrow ingression. Cellular contractility is further regulated by the cortexillin-binding IQGAP proteins, providing tunability to the mechanosensory system. However, how these proteins interact at a molecular level to affect mechanosensory responses remains unknown.

In this study, we examined the dynamics and mobility of key mechanoresponsive proteins using fluorescence recovery after photobleaching (FRAP) and fluorescence correlation spectroscopy (FCS) to understand how they are recruited to and retained at the cleavage furrow. We observed that the mechanoresponsive proteins, including myosin II, cortexillin I and IQGAP2, show marked reduction in mobility at the cleavage furrow compared to the interphase cortex. This indicates that these proteins are forming stable complexes at the furrow. Further, the shift in protein mobility at the furrow is driven by mechanical stress, and is robust to many genetic perturbations. In addition, we used proteomics to identify protein-protein interactions important for mechanoresponsiveness. We found that myosin II can associate with both cortexillin I and IQGAP2, further suggesting the existence of large scale assemblies of

mechanoresponsive complexes. Thus, this study gives new insight into how different cytoskeletal elements can work together to respond to mechanical stress, and regulate contractility during cytokinesis.

3.1. Equatorial proteins have slower recovery times than polar crosslinkers, and exhibit reduced mobility at the cleavage furrow

The short time-scale dynamics of proteins regulate their recruitment and localization. Actin-associated proteins may be classified into two groups – the equatorially enriched cleavage furrow proteins and the polar or globally distributed proteins ([27], **Fig. 3.1A**). We used fluorescence recovery after photobleaching (FRAP) to examine the dynamics of these groups in interphase and dividing *Dictyostelium* cells, and to explain differences in their spatiotemporal localization. We measured the fluorescence intensity in the bleached region until the recovery curve saturated (10-25 s), allowing accurate calculation of recovery times and immobile fractions for key cytoskeletal proteins (**Fig. 2.3**). The characteristic recovery time is dominated by binding-unbinding rates, while the immobile fraction represents the population that does not turn over during the experiment (**Fig. 3.1B**). As *Dictyostelium* cells are highly motile, longer acquisitions can show additional long-scale recovery due to cellular motility instead of protein dynamics. Thus, for this study we only measure the fast dynamic recovery and mobility. In interphase cells, GFP-actin recovers within a second, establishing the dynamicity of the actin network (**Fig. 3.1C, D, Table 2**). The cortical actin recovery times and immobile fractions were significantly higher than for GFP or cytoplasmic GFP-actin (**Fig. 3.1C, 1D**). Thus, the

cortical FRAP measurements report on the dynamics of the cortical cytoskeletal network, even though $\sim 70\%$ of the total actin ($250 \mu\text{M}$) in *Dictyostelium* cells is monomeric [39].

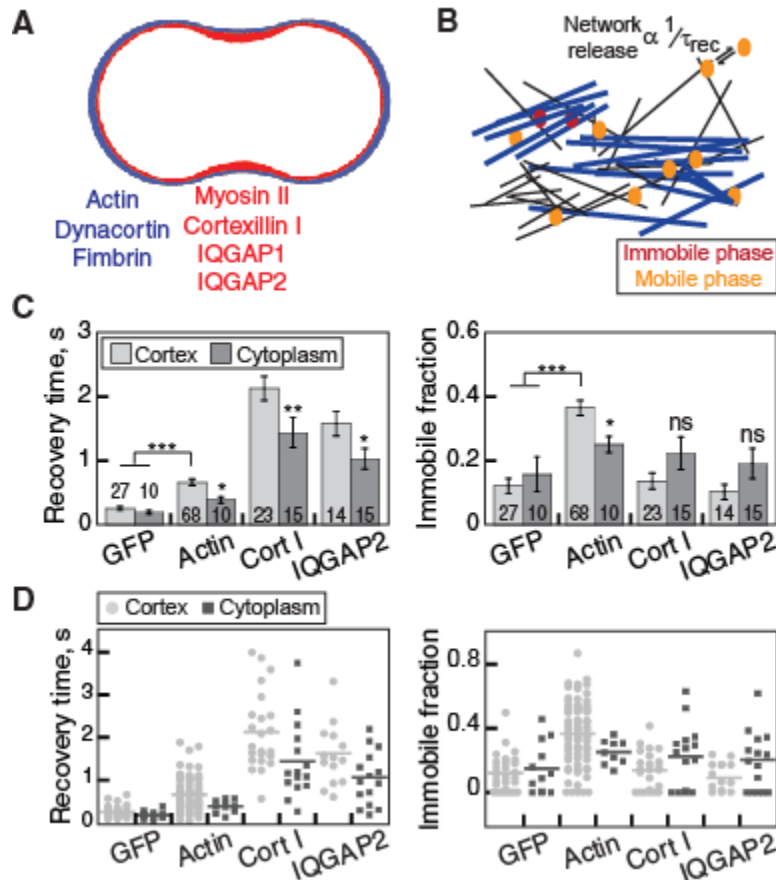


Figure 3.1: Cytoskeletal protein dynamics measured by FRAP. (A) Cytoskeletal proteins are asymmetrically localized during cytokinesis. (B) From FRAP analysis, the network release rate is inversely proportional to the recovery time (τ), while the immobile fraction (dark red circles) represents the protein population that does not turnover during the experiment. The protein mobile fraction is represented by light orange circles. The thick and thin lines represent the immobile and mobile populations of actin, respectively. (C) Recovery times and immobile fractions for soluble GFP and cytoskeletal proteins at the cell cortex and in the cytoplasm in interphase cells as measured by FRAP. Cytoskeletal proteins show slower recovery in the cortex than in the cytoplasm. (D) Distribution of recovery times and immobile fractions for soluble GFP and cytoskeletal proteins at the cell cortex and in the cytoplasm. Asterisks represent the significance of difference between interphase and furrow measurements where ns: $p > 0.05$, *: $p < 0.05$, **: $p < 0.005$, ***: $p < 0.0005$ based on ANOVA with Fischer's LSD post-test.

Genetic, biochemical and mechanical studies have demonstrated cross-talk between the polar and equatorial modules [3, 16]. However, how these proteins interact dynamically to control these processes is unknown. Here, we study the dynamics of proteins important for cytokinesis to develop a mechanistic understanding of how cells divide and regulate their shape. This would provide insight into how the fast molecular events governing cytokinesis, including motor activity, actin filament turnover and rearrangement, and crosslinker interactions, regulate much slower cell shape changes.

Interestingly, we observed that actin dynamics changed during cytokinesis as the recovery time increased and the immobile fraction decreased in the furrow (**Fig. 3.2, Table 2**). In comparison, the dynacortin and fimbrin recovery times at the furrow increased significantly, while their mobility was unaffected (**Fig. 3.2, [27]**). The polar cortex dynamics of dynacortin and fimbrin were similar to interphase values, while actin showed increased mobility at the poles (data not shown). Myosin II, cortexillin I and IQGAP2, which localize to the cleavage furrow, recovered more slowly (1.5-5 s) than actin or polar crosslinkers in the interphase cortex (**Fig. 3.2, Table 2**). Their much slower recovery than that of soluble GFP demonstrates that the fluorescence recovery is dominated by unbinding events at the cortex instead of diffusion. Further, their cytoplasmic recovery times are significantly faster than those in the cortex (**Fig. 3.1C, D**), indicating that the equatorial proteins form stable complexes at the cortex with slower unbinding. Cortexillin I recovery was slower at the furrow than in interphase, while myosin II and IQGAP2 showed no change. In contrast, myosin II recovery slows in anaphase as compared to metaphase in *Drosophila* S2 cells [40].

The equatorial proteins had high mobility during interphase compared to other proteins (**Fig. 3.2**). The mobility of cortexillin I and IQGAP2 in the interphase cortex were comparable to those in the cytoplasm (**Fig. 3.1C, D**). However, the immobile fractions for these proteins increased significantly at the cleavage furrow (**Fig. 3.2, Table 2**). The magnitude of mobility shift for cortexillin I and IQGAP2 was higher than for myosin II [16, 27, 41]. Thus, we focused on cortexillin I and IQGAP2 dynamics for the remainder of this study. The reduction in protein mobility at the furrow suggests that these proteins are stabilized at the cortex during furrow ingression, consistent with their slower recovery times. The high immobile fractions also likely promote their furrow enrichment. Therefore, determining the factors that cause this mobility shift is essential to explaining how the contractile proteins accumulate and remodel during furrow ingression.

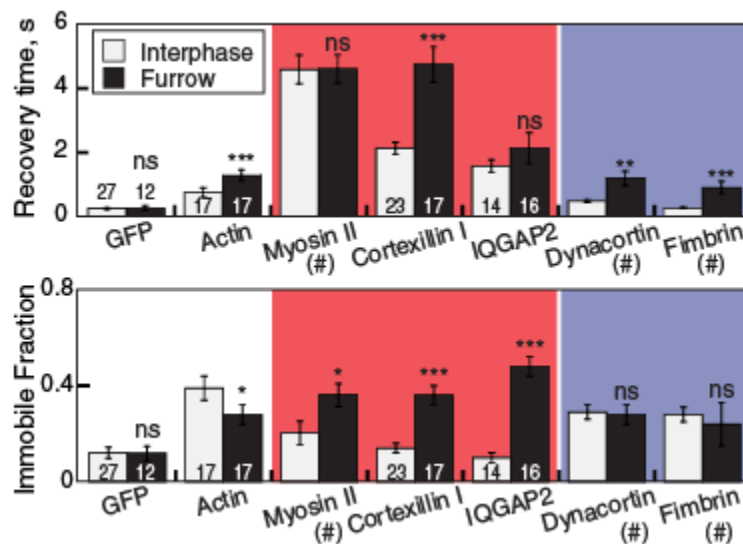


Figure 3.2: Changes in cytoskeletal protein dynamics during cytokinesis. Recovery times and immobile fractions of different cytoskeletal proteins in the interphase cortex and at the cleavage furrow. Equatorially enriched proteins – myosin II, cortexillin I and IQGAP2 – have markedly reduced mobility at the cleavage furrow. Values plotted are mean \pm SEM; sample sizes are listed on the bars (see **Table 3.1**). Asterisks represent the significance of difference between interphase and furrow measurements where ns: $p > 0.05$, *: $p < 0.05$, **: $p < 0.005$, ***: $p < 0.0005$ based on ANOVA with Fischer's LSD post-test. #: FRAP data for myosin II is reproduced from [16] and for dynacortin and fimbrin from [27].

3.2. Genetic control of protein dynamics is suppressed at the furrow

Previous genetic studies established the functional interplay between myosin II, cortexillin I, and the IQGAPs in governing protein accumulation and contractility at the cleavage furrow and in responding to mechanical stress [25] (**Fig. 3.3A**). Thus, we tested whether the same genetic relationships also dictate protein dynamics, regulating their furrow accumulation. We conducted FRAP on cortexillin I and IQGAP2 at the interphase cortex and the furrow in cell lines lacking key components of this mechanoresponsive system (**Fig. 3.3B**).

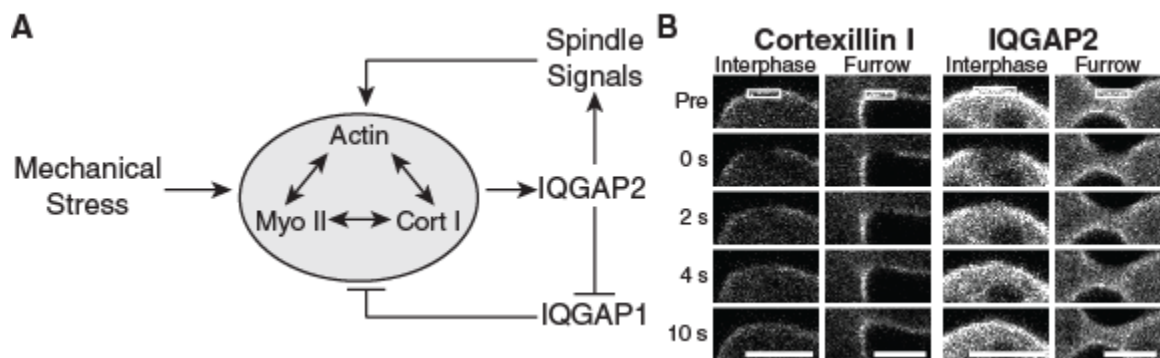


Figure 3.3: Cortexillin I and IQGAP2 dynamics at the cleavage furrow. (A) A myosin II-cortexillin I-actin-based mechanosensory system regulates contractility at the furrow, and IQGAP proteins regulate accumulation of the contractile proteins. (B) Confocal images showing photobleaching and fluorescence recovery of GFP-cortexillin I and GFP-IQGAP2 in the cortex of interphase cells and at the cleavage furrow. Scale bar is 5 μ m.

Cortexillin I recovery time increased at the furrow compared to the interphase cortex in wild type (WT) cells (**Fig. 3.4A, C, Table 2**). However, this slower recovery was not observed in *myosin II* (*myoII*) and *iqgap2* (*iqg2*) null cells (**Fig. 3.4A, C, Table 2**). In contrast, while IQGAP2's recovery time was unaltered at the furrow in WT cells, IQGAP2 had significantly higher recovery time at the furrow in *myoII* cells (**Fig. 3.4B, D, Table 2**). Both cortexillin I and IQGAP2 had >2-fold higher immobile fractions at the

cleavage furrow (**Fig. 3.4A-D, Table 2**). Cortexillin I immobile fractions were higher in interphase *myoII* and *iqg2* compared to WT, but were unchanged at the furrow in these mutants (**Fig. 3.4A, C, Table 2**). This demonstrates that while myosin II and IQGAP2 are important for maintaining a mobile pool of cortexillin I, additional factors such as mechanical stress could dominate cortexillin I mobility at the furrow, ensuring its recruitment during cytokinesis, as cortexillin I also shows mechanical stress-dependent accumulation [6, 25]. Consistently, the cleavage furrow localization of cortexillin I was not affected in any of the mutants tested. IQGAP2 immobile fraction was also higher in interphase *myoII* as compared to WT (**Fig. 3.4B, D, Table 2**), suggesting that myosin II drives the dynamic remodeling of the cytoskeletal network. Myosin II's full power stroke is required for this mobility regulation, as the 10-fold slower S456L mutant myosin II, which only takes a 2-nm step (1/4 of WT) [6, 27, 42], fails to rescue the IQGAP2 and cortexillin I mobility defects seen in *myoII* cells (**Fig. 3.5**). Although myosin II regulates the actin cortex dynamics in epithelial cells [43, 44], deletion of myosin II, cortexillin I or IQGAP2 had no impact on actin dynamics (**Fig. 3.6**).

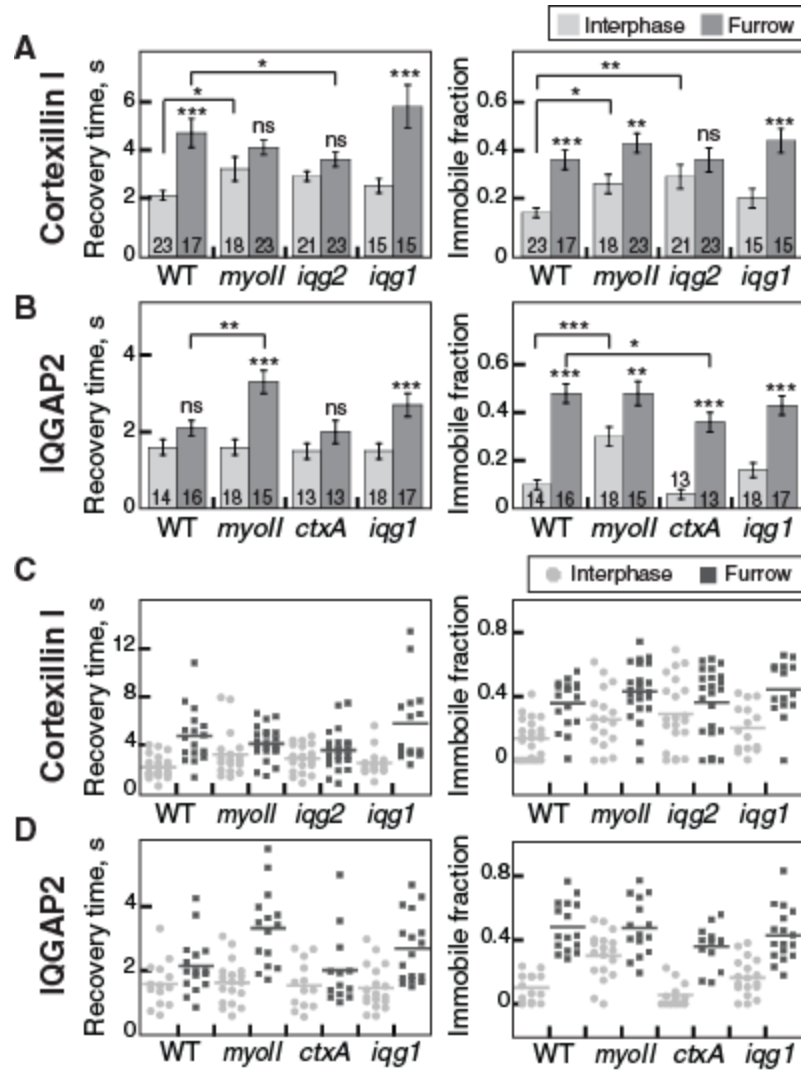


Figure 3.4: Changes in cortexillin I and IQGAP2 dynamics at the cleavage furrow in genetic mutants. (A, B) Recovery times and immobile fractions for GFP-cortexillin I (A) and GFP-IQGAP2 (B) in different genetic mutants in the cortex of interphase and dividing cells. (C, D) Distribution of recovery times and immobile fractions for GFP-cortexillin I (C) and GFP-IQGAP2 (D) in different genetic mutants in interphase and dividing cells. Values plotted are mean \pm SEM; sample sizes are listed on the bars (see Table 2). p values represented as ns: $p > 0.05$, *: $p < 0.05$, **: $p < 0.005$, ***: $p < 0.0005$ based on ANOVA with Fischer's LSD post-test. Asterisks above the furrow measurement represent significance of difference from interphase values. Comparisons across mutants are represented by asterisks above the connecting lines.

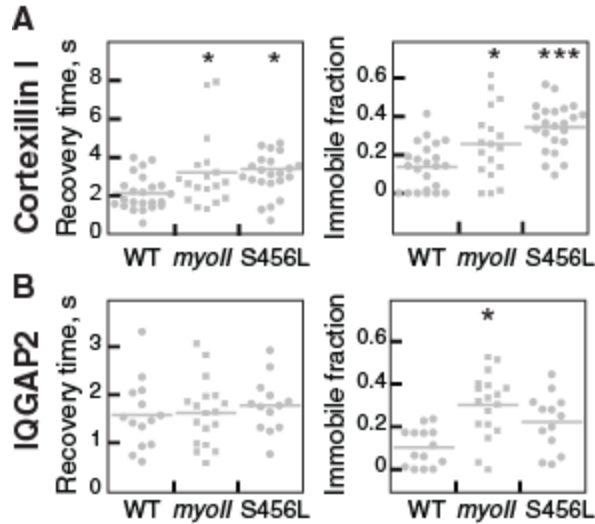


Figure 3.5: Effect of myosin II motor activity on cortexillin I and IQGAP2 dynamics. Distribution of recovery times and immobile fractions for GFP-cortexillin I (**A**) and GFP-IQGAP2 (**B**) in WT, *myoII* and S456L *myoII* cells. *p* values are represented as ns: $p > 0.05$, *: $p < 0.05$, **: $p < 0.005$, ***: $p < 0.0005$ based on ANOVA with Fischer's LSD post-test.

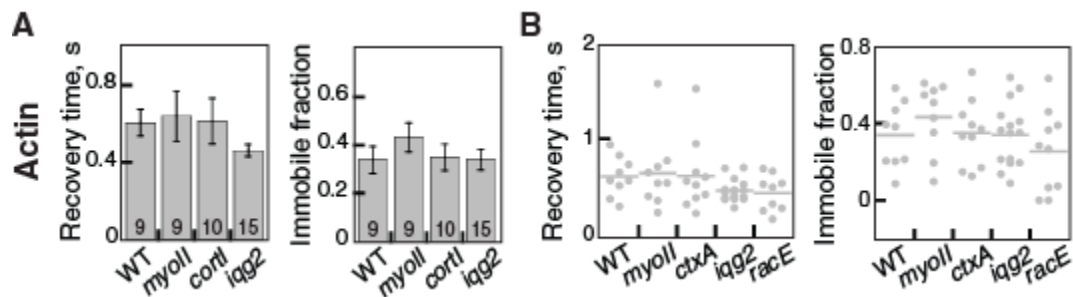


Figure 3.6: Actin dynamics are unchanged in different genetic mutants (**A**) Recovery times and immobile fractions for GFP-actin in different genetic mutants in the interphase cortex. (**B**) Distribution of recovery times and immobile fractions of GFP-actin in the interphase cortex of different mutants. Values plotted are mean \pm SEM; sample sizes are listed on the bars (See **Table 2**).

The deletion of IQGAP1 (*iqg1*) did not affect the interphase or furrow dynamics of either cortexillin I or IQGAP2 (**Fig 3.4, Table 2**), in agreement with its role as a damper of stress-dependent protein accumulation [25]. Because IQGAP1 and IQGAP2 interact with distinct domains of cortexillin I [34, 45, 46], we also studied cortexillin I dynamics in the *iqg1/2* double mutant. Here, cortexillin I still showed faster recovery at the furrow as compared to WT, similar to *iqg2* (**Fig. 3.7, Table 2**). However, the immobile fraction at

the furrow was higher in the double mutant compared to the WT or *iqg2* mutant (**Fig. 3.7, Table 2**). The *iqg1/2* cells show enhanced stress-dependent protein accumulation, while *iqg2* cells are unresponsive due to IQGAP1 inhibition [25]. Thus, the reduced mobility of cortexillin I at the furrow is likely due to mechanical stresses locking in the cytoskeletal network of these highly mechanoresponsive cells.

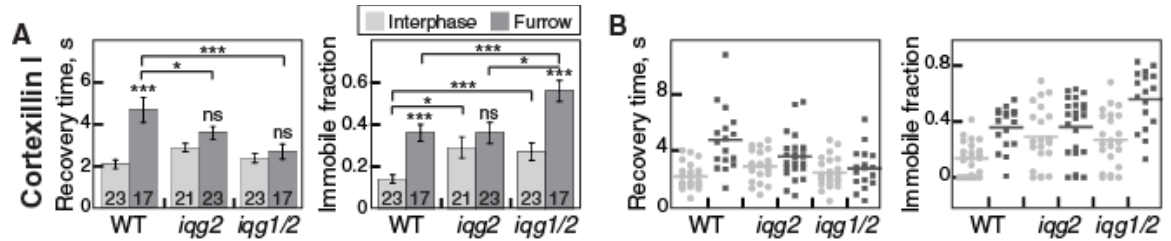


Figure 3.7: IQGAP2 affects cortexillin I dynamics (A) Mean recovery times and immobile fractions for GFP-cortexillin I in WT, *iqg2* single, and *iqg1/2* double mutants. **(B)** Distribution of recovery times and immobile fractions for GFP-cortexillin I in WT, *iqg2* single, and *iqg1/2* double mutants. Values plotted are mean \pm SEM; sample sizes are listed on the bars (See **Table 2**). *p* values are represented as ns: $p > 0.05$, *: $p < 0.05$, **: $p < 0.005$, ***: $p < 0.0005$ based on ANOVA with Fischer's LSD post-test.

To examine molecular scale events driving the protein dynamics changes, we used fluorescence correlation spectroscopy (FCS) to measure the *in vivo* diffusion of cortexillin I and IQGAP2 across various mutant backgrounds. FCS experiments were performed in the cytoplasm as cell movement precluded positioning the confocal volume at the cortex. We compared the diffusion time for cortexillin I and GFP in the cytoplasm to that of purified proteins *in vitro*. GFP had 5-fold reduction in diffusion time in cells while cortexillin I showed >8-fold slower diffusion (**Fig. 3.8A, Table 4**), confirming that cortexillin I is a part of large molecular assemblies. The deletion of myosin II did not impact the cytoplasmic diffusion of either cortexillin I or IQGAP2 though it increased the immobile fraction of both proteins at the cortex (**Fig. 3.8B, C**), implying that myosin II affects protein dynamics by regulating contractility and cytoskeletal structure. The diffusion time for cortexillin I was increased by ~30% in *iqg2* cells (**Fig. 3.8B, Table 4**).

This suggests that without IQGAP2, the effective mass of the cortexillin I complex roughly doubles as diffusion time is approximately proportional to the cube root of the effective molecular weight of the diffusing species. As expected, cortexillin I diffusion also showed a similar trend in the *iqg1/2* double mutant (Fig. 3.8B, Table 4). Thus, the changes in cortexillin I mobility could arise from changes in biochemical interactions in the absence of IQGAP2.

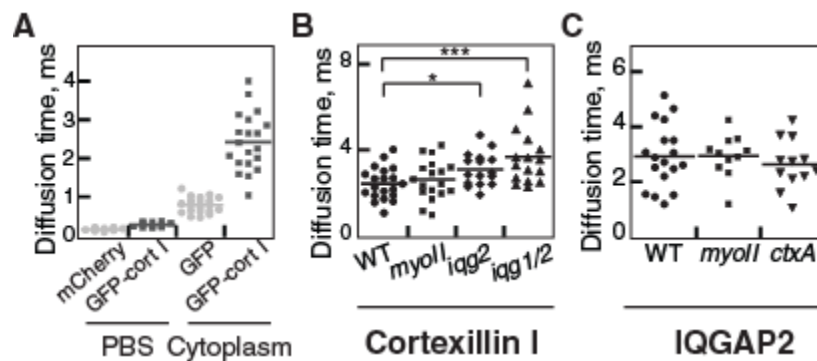


Figure 3.8: Diffusion times for cortexillin I and IQGAP2 measured by FCS (A) Diffusion times for purified mCherry and GFP-cortexillin I *in vitro*, and GFP and GFP-cortexillin I in cellular cytoplasm as measured by FCS. (B, C) Cytoplasmic diffusion times measured by FCS for GFP-cortexillin I (B) and GFP-IQGAP2 (C) in different mutants. Calculated diffusion coefficients are provided in Table 4. *p* values are represented as ns: $p > 0.05$, *: $p < 0.05$, **: $p < 0.005$, ***: $p < 0.0005$ based on ANOVA with Fischer's LSD post-test.

Collectively, the FRAP and FCS experiments enabled us to attribute changes in cortexillin I mobility to either protein-protein interactions (in *iqg2* and *iqg1/2*) or cortex re-structuring (in *myoII*). We demonstrated that the dynamics of cortexillin I and IQGAP2 at the cleavage furrow are well conserved across mutants, though differences emerge during interphase (Fig. 3.9). As cleavage furrow contractility is common to all cells, we hypothesized that mechanical stresses acting at the furrow could override the biochemical signals to define cleavage furrow protein dynamics. Physical mechanisms such as myosin II-mediated force generation, Laplace pressure-mediated furrow thinning,

and protrusive forces from the polar cortex drive furrow ingression [9]. Thus, we next examined whether mechanical stresses at the cleavage furrow were sufficient to shift the dynamics of these mechanoresponsive proteins.

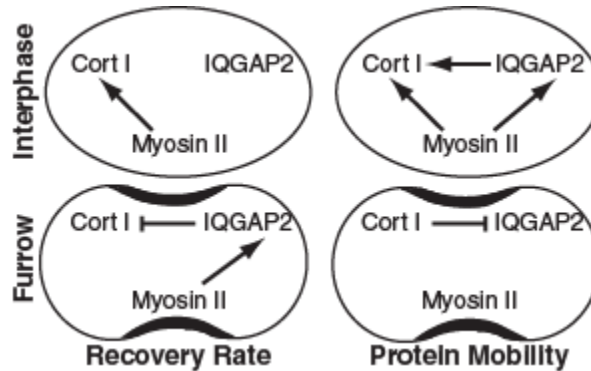


Figure 3.9: Schematic showing the effect of key cytoskeletal proteins on the dynamics of cortexillin I and IQGAP2, based on FRAP measurements.

3.3. Mechanical stress drives the reduction in cleavage furrow mobility of cortexillin I and IQGAP2

In addition to enrichment at the cleavage furrow, myosin II, cortexillin I and IQGAP2 accumulate to sites of externally applied mechanical stress, thereby allowing the cell to retract against this stress [6, 24, 25]. Hence, we applied compression using agarose overlay to test if mechanical stress, as compared to biochemical signaling, affects protein dynamics changes at the cleavage furrow. Flattening of the cells drives the accumulation of the mechanoresponsive proteins studied here to the cell cortex to counter the compressive stress [25, 28]. The ratio of fluorescence intensity in the cortex to that in the cytoplasm is dependent on the thickness of agarose and plating density (T. Luo and Robinson, unpublished data), confirming that the increase in cortical intensity is driven

by mechanical stress and is not simply due to volume effects. Further, soluble GFP does not change in cortical intensity upon compression [25].

We examined cortexillin I and IQGAP2 interphase dynamics in presence or absence of compression across mutants studied above (**Fig. 3.10, Table 2**). Cortexillin I exhibited a slower recovery time under compression, but IQGAP2's recovery time was unaffected (**Fig. 3.11A-D**). Both cortexillin I and IQGAP2 showed a >2-fold increase in the immobile fraction under compression (**Fig. 3.11**), similar to the observation at the furrow (**Fig. 3.4**). By FCS, the cortexillin I diffusion time also doubled under compression, while IQGAP2 diffusion was unaffected (**Fig. 3.13, Table 4**). Both the recovery time and immobile fraction for IQGAP2 increased in compressed *myoII* compared to WT (**Fig. 3.11B, D, 3.12, Table 2**). Cortexillin I and IQGAP2 dynamics under compression did not change in other mutants as compared to WT (**Fig. 3.11, 3.12, Table 2**). The cortexillin I mobility shift in *iqg2* cells under compression was higher than that observed at the furrow (**Fig. 3.11A, 3.4A**), suggesting that under compression cortexillin I directly responds to mechanical stress, compared to the cleavage furrow where biochemical signals through IQGAP2 also contribute to cortexillin I mobility. Importantly, both compression and cleavage furrow showed a consistent, >2-fold increase in immobile fractions of both cortexillin I and IQGAP2 compared to the unstressed, interphase cortex across various mutants (**Fig. 3.4, 3.11**). This validates the importance of mechanical stress in driving the dynamics of equatorially enriched proteins at the cleavage furrow, thereby ensuring their robust localized accumulation.

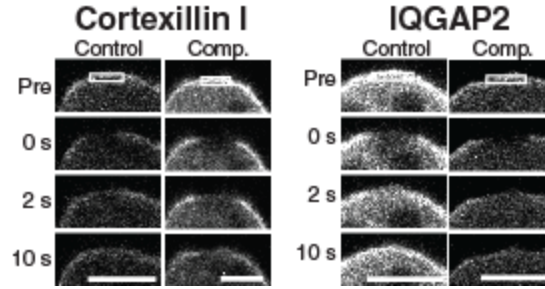


Figure 3.10: Changes in cortexillin I and IQGAP2 dynamics upon compression. Confocal images showing photobleaching and fluorescence recovery of GFP-cortexillin I and GFP-IQGAP2 in the cortex of interphase uncompressed and compressed cells. Scale bar is 5 μ m.

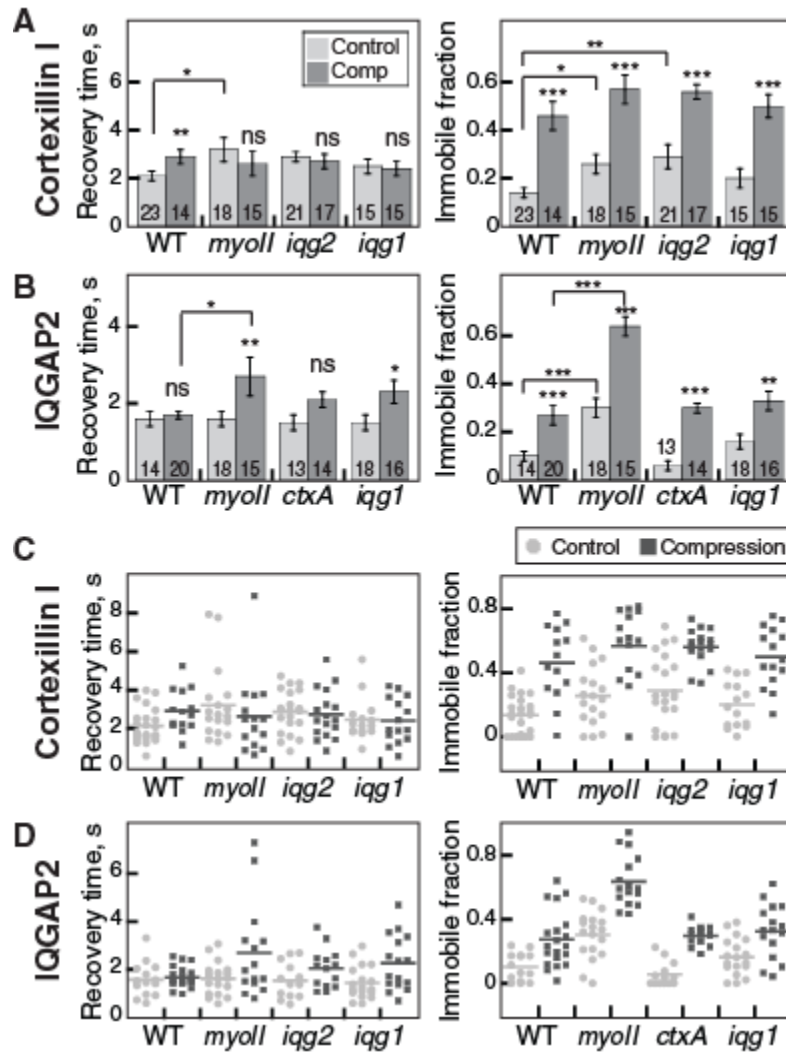


Figure 3.11: Changes in cortexillin I and IQGAP2 dynamics upon compression in genetic mutants. (A, B) Recovery times and immobile fractions for GFP-cortexillin I (A) and IQGAP2 (B) in different genetic mutants in absence or presence of compressive stress. (C, D) Distribution of recovery times and immobile fractions for GFP-cortexillin I (C) and IQGAP2 (D) in different genetic mutants in absence or presence of compressive stress. Values plotted are mean \pm SEM; sample sizes are listed on the bars (See **Table 2**). *p* values are represented as ns: *p* > 0.05, *: *p* < 0.05, **: *p* < 0.005, ***: *p* < 0.0005 based on ANOVA with Fischer's LSD post-test.

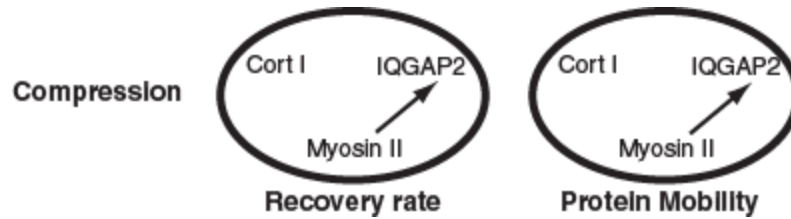


Figure 3.12: Schematic showing the effect of key cytoskeletal proteins on the dynamics of cortexillin I and IQGAP2 under compression, based on FRAP measurements.

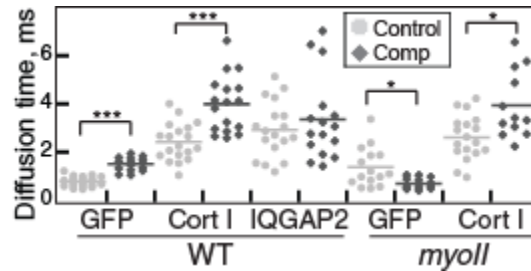


Figure 3.13: Protein diffusion under compression. Diffusion times for GFP, cortexillin I and IQGAP2 measured by FCS in WT and *myoII* cells. Calculated diffusion coefficients are provided in **Table 4**. *p* values are represented as ns: $p > 0.05$, *: $p < 0.05$, **: $p < 0.005$, ***: $p < 0.0005$ based on ANOVA with Fischer's LSD post-test.

In addition, by measuring dynamics of cortexillin I and IQGAP2 in cells lacking the small GTPase *racE* (*racE*), we assessed the contribution of cortical tension on protein dynamics, as *racE* is a major regulator of cortical mechanics [21, 27, 30]. For cortexillin I, the immobile fraction was higher and the recovery time was shorter in *racE* cells, while IQGAP2 dynamics were unchanged (**Fig. 3.14**). Thus, cortexillin dynamics are not only affected by mechanical stress but also by general cortical mechanics. Furthermore, the mobility and recovery times of GFP-actin were not affected by compression. Overall, cortexillin I dynamics are more sensitive to compressive stresses than the dynamics of IQGAP2, actin and GFP are.

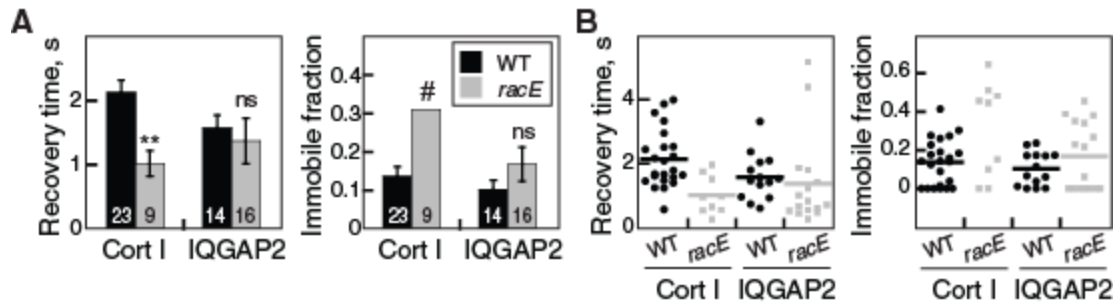


Figure 3.14: The effect of RacE on cortexillin I and IQGAP2 dynamics. (A) Average recovery times and immobile fractions of GFP-cortexillin I and GFP-IQGAP2 in WT and *racE* null cells. (B) Distribution of recovery times and immobile fractions of GFP-cortexillin I and GFP-IQGAP2 in WT and *racE* null cells. Values plotted are mean \pm SEM; sample sizes are listed on the bars. *p* values are represented as ns: $p > 0.05$, *: $p < 0.05$, **: $p < 0.005$, ***: $p < 0.0005$ based on ANOVA with Fischer's LSD post-test. #: The immobile fraction for cortexillin I in *racE* null cells is bimodal (see panel B); hence SEM is not shown.

As compression reduced cell height by up to 4-fold, we measured GFP dynamics to examine the impact of altered protein transport and cellular structure upon compression. The immobile fraction and diffusion time for GFP nearly doubled (Fig. 3.15, 3.13), suggesting sieving effects may become significant under compression. The altered GFP dynamics under compression confirm that network structure and intracellular environment are important contributors to mechanical stress-dependent protein dynamics. However, in *myoII* cells, GFP FRAP dynamics did not change upon compression, rather GFP diffusion was faster in compressed *myoII* cells (Fig. 3.15, 3.13), suggesting that myosin II is important for stabilizing the cortex under mechanical stress, and in its absence the cortical dynamics are dominated by passive diffusive behaviors [47]. As the actin cytoskeleton forms a highly dense meshwork in *Dictyostelium*, structural changes between interphase and furrow cortex cannot be resolved by confocal and electron microscopy [27]. Thus, we next chemically perturbed the cytoskeleton to determine how these network properties affect protein mobility and dynamics.

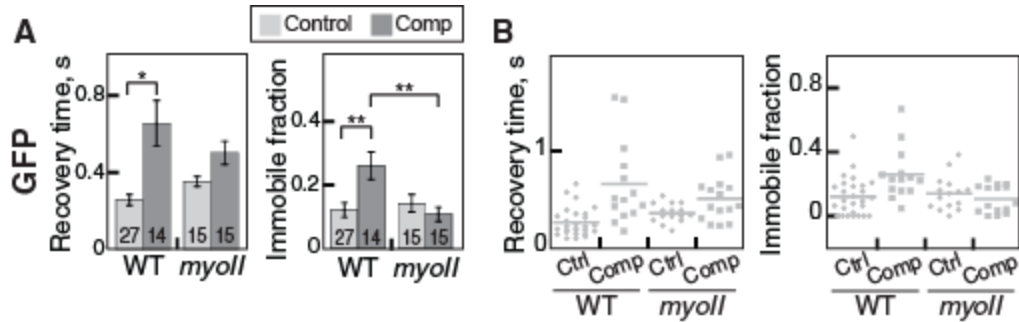


Figure 3.15: GFP dynamics under compression. (A) Average recovery time and immobile fraction for GFP in WT and *myoII* cells. (B) Distribution of recovery time and immobile fraction for GFP in WT and *myoII* cells. Values plotted are mean \pm SEM; sample sizes are listed on the bars (See **Table 2**). *p* values are represented as ns: $p > 0.05$, *: $p < 0.05$, **: $p < 0.005$, ***: $p < 0.0005$ based on ANOVA with Fischer's LSD post-test.

3.4. Alterations to cortical structure and mechanics shift mobility of cortexillin I

To test the effect of cytoskeletal structure on protein dynamics, we perturbed the actin cytoskeleton by treating the cells with either latrunculin-A or jasplakinolide.

Latrunculin-A prevents F-actin assembly by sequestering free G-actin monomers, while jasplakinolide enhances actin filament nucleation. We quantified changes in F-actin amount upon treatment with latrunculin-A and jasplakinolide by measuring the relative fluorescence intensity of cells stained with phalloidin 15-minutes post-drug treatment [5] (**Fig. 3.16**). Anti-actin staining was also used to visualize changes in actin level and cytoskeletal morphology (**Fig. 3.16**). Interestingly, even with 5 μ M latrunculin-A, cells still had ~50% residual F-actin (~35 μ M) (**Fig. 3.16B**), suggesting sufficient F-actin binding sites for the ~1 μ M actin crosslinkers [28, 48, 49]. The residual F-actin mostly concentrated in puncta illustrating discontinuity of the cytoskeletal network (**Fig. 3.16A**). Latrunculin-A had a drastic effect on cellular mechanics, as 1 μ M latrunculin-A-treated cells had 12-fold lower cortical tension as measured by micropipette aspiration (**Fig. 3.17**), consistent with the 85% reduction in viscoelasticity previously reported for

latrunculin-B treatment [26]. 5 μM latrunculin-A-treated cells were too soft for mechanical measurements. In contrast, jasplakinolide enhanced the cellular F-actin levels ~ 4 -fold inducing the formation of F-actin clusters (**Fig. 3.16**), and increased cortical tension slightly (**Fig. 3.17**). Jasplakinolide also increased the recovery time of soluble GFP while not affecting its immobile fraction or diffusion (**Fig. 3.18**). The discontinuity of the cytoskeleton upon latrunculin-A treatment is also reflected by the increase in the recovery time and immobile fraction of GFP even though its diffusion is unaffected (**Fig. 3.18**). Thus, we were able to directly probe the impact of changes in cytoskeletal structure and mechanics on protein dynamics by using these two compounds.

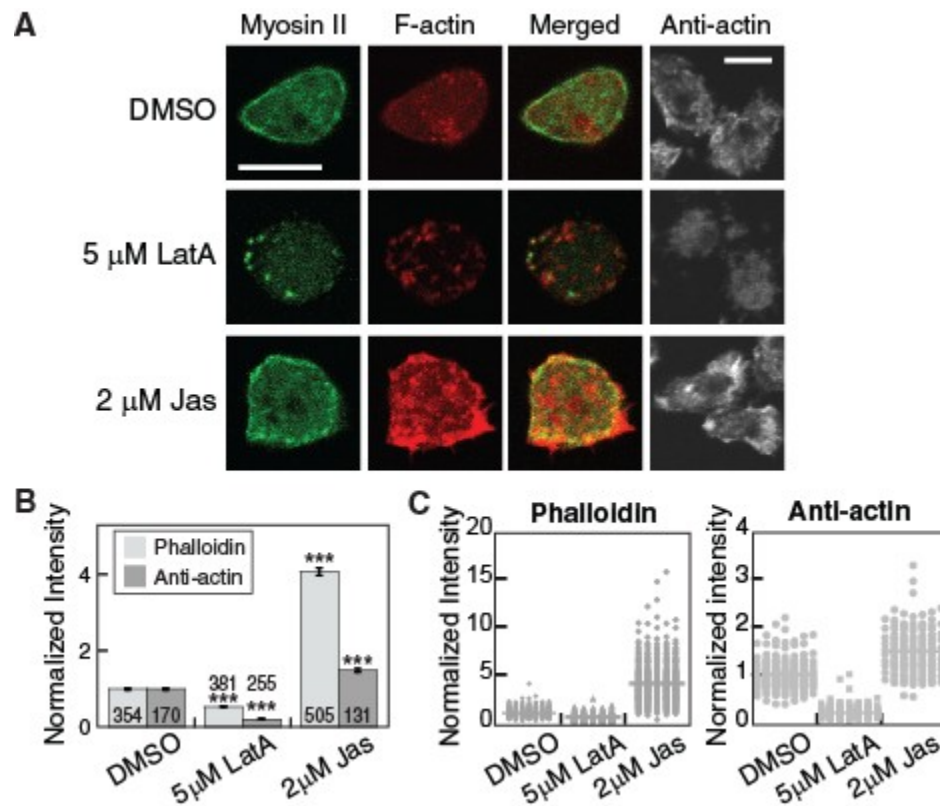


Figure 3.16: Perturbation of actin cytoskeleton by latrunculin-A and jasplakinolide. (A) Confocal images of TRITC-phalloidin-stained GFP myosin II expressing cells and anti-actin stained cells show changes in the cytoskeletal architecture 15 minutes post-treatment with 5 μM latrunculin-A or 2 μM jasplakinolide. (B) Quantification of relative F-actin amount based on the fluorescence intensity of TRITC-phalloidin and anti-actin staining. (C) Distribution of normalized fluorescence intensity of TRITC-phalloidin and anti-actin staining.

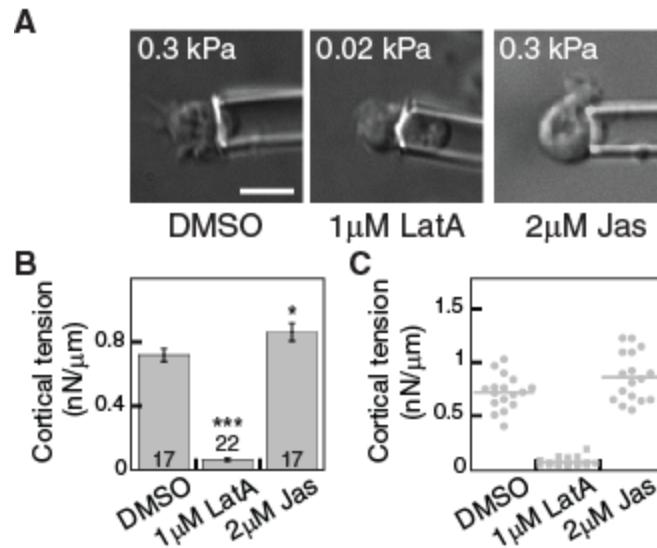


Figure 3.17: Effect of latrunculin-A and jasplakinolide on cell mechanics (A) DIC images of micropipette aspiration experiments with DMSO, 1 μM latrunculin-A and 2 μM jasplakinolide (B) Cortical tension measurements for DMSO, 1 μM latrunculin-A and 2 μM jasplakinolide-treated cells measured by micropipette aspiration (C) Distribution of cortical tension measured by micropipette aspiration on cells treated with DMSO, 1 μM latrunculin-A or 2 μM jasplakinolide.

Latrunculin-A or jasplakinolide treatment did not significantly affect cortexillin I recovery time, but both compounds appreciably increased its immobile fraction (**Fig. 3.18A, B, Table 3**). Latrunculin-A also increased the recovery time and immobile fraction of IQGAP2 (**Fig. 3.18A, B, Table 3**). IQGAP2 diffusion was insensitive to both drugs (**Fig. 3.18C, Table 4**). However, cortexillin I showed two differently diffusing populations with latrunculin-A treatment – one with a similar diffusion time as the control (~ 2 ms) and another much slower population (~ 8 ms) (**Fig. 3.18C, Table 4**). This slower population likely reflects the diffusion of cortexillin I in actin clusters observed upon F-actin staining. Though jasplakinolide treatment promoted F-actin cluster formation, its effect on protein dynamics was not as pronounced (**Fig. 3.18, Tables 3-4**). These results demonstrate that the connectivity of the cytoskeleton network is extremely important for maintaining normal protein dynamics. Remarkably, cortexillin I remained

localized at the furrow in latrunculin-A-treated cells, though its distribution was non-uniform (**Fig. 3.19A**). Its recovery time and mobility in the furrow were unaffected by latrunculin-A (**Fig. 3.19B, C**). Thus, the cortexillin I immobile fraction under mechanical stress is either saturated or becomes independent of network structure. In contrast, myosin II completely lost its cortical localization upon latrunculin-A treatment and formed puncta throughout the cell (**Fig. 3.16A**) [5].

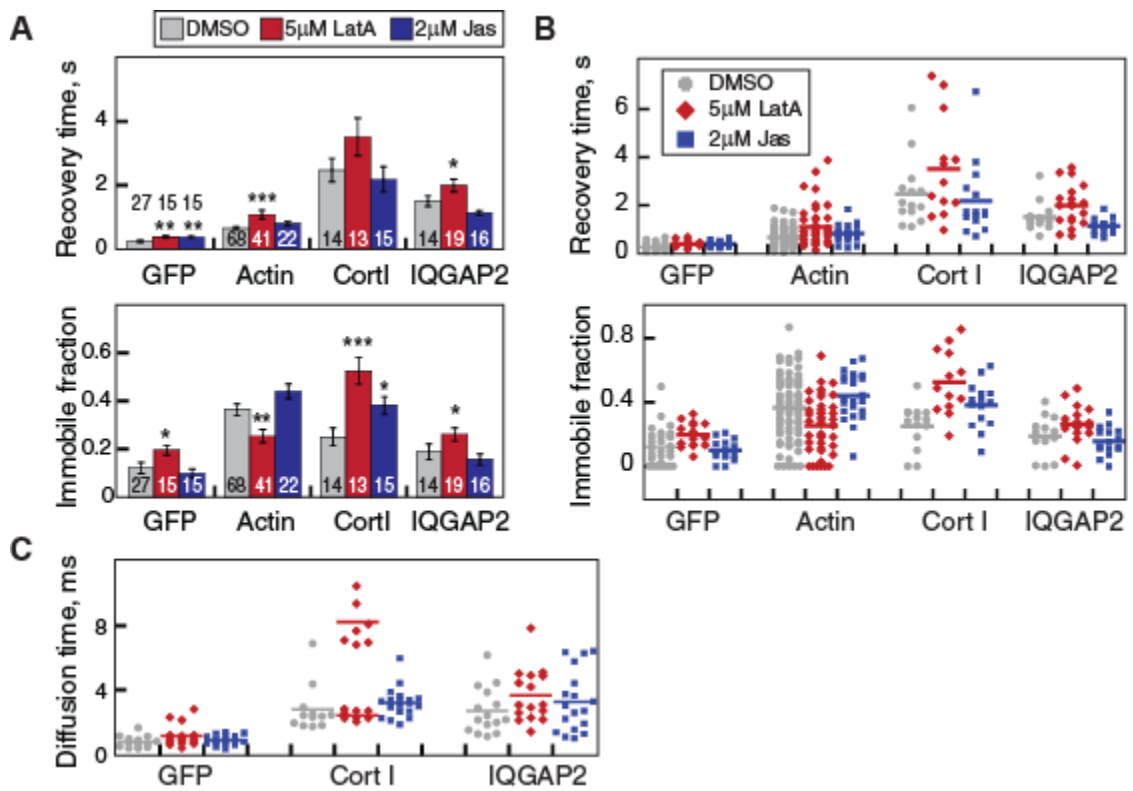


Figure 3.18: Effect of latrunculin-A and jasplakinolide on protein dynamics. (A) Recovery times and immobile fractions of soluble GFP, GFP-actin, GFP-cortexillin I and GFP-IQGAP2 in untreated, 5 μ M latrunculin A or 2 μ M jasplakinolide treated cells as measured by FRAP (see **Table 3**). (B) Distribution of recovery times and immobile fractions for GFP, GFP-actin, GFP-cortexillin I and GFP-IQGAP2 in DMSO, 5 μ M latrunculin-A or 2 μ M jasplakinolide-treated cells. (C) Diffusion times for GFP, GFP-cortexillin I and GFP-IQGAP2 in untreated, 5 μ M latrunculin-A or 2 μ M jasplakinolide treated cells as measured by FCS (see **Table 4**). Cortexillin I shows two differently diffusing populations upon latrunculin-A treatment, while the diffusion of GFP and IQGAP2 is unaffected by the pharmacological treatment. Values plotted are mean \pm SEM; sample sizes are listed on the bars. Asterisks represent significance of difference from DMSO control, where p values represented as ns: $p > 0.05$, *: $p < 0.05$, **: $p < 0.005$, ***: $p < 0.0005$ based on ANOVA with Fischer's LSD post-test.

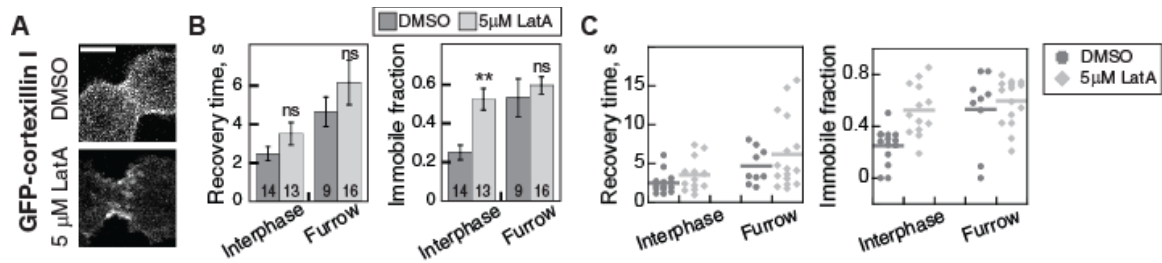


Figure 3.19: Effect of latrunculin-A on cortexillin I dynamics in dividing cells. (A) Confocal images showing cleavage furrow recruitment of GFP-cortexillin I in untreated and 5 μM latrunculin-A-treated cells. (B) Recovery times and immobile fractions of GFP-cortexillin I in interphase and dividing cells with or without 5 μM latrunculin-A treatment. (C) Distribution of recovery times and immobile fractions of GFP-cortexillin I in interphase and dividing cells with or without 5 μM latrunculin-A. Values plotted are mean \pm SEM; sample sizes are listed on the bars. Asterisks represent significance of difference from DMSO control, where p values represented as ns: $p > 0.05$, *: $p < 0.05$, **: $p < 0.005$, ***: $p < 0.0005$ based on ANOVA with Fischer's LSD post-test.

Latrunculin-A also increased actin mobility and recovery rate, while jasplakinolide had no effect (Fig. 3.18A, B). The increased actin mobility with latrunculin-A is quantitatively similar to that at the furrow (Fig. 3.18A, 3.2), further validating the importance of cytoskeletal restructuring during cytokinesis (Fig. 3.20). These dynamic features also explain why actin does not show a significant accumulation at the cleavage furrow or upon micropipette aspiration [27, 28]. Overall, perturbations to the cytoskeletal structure are sufficient to affect changes in the dynamics of cytoskeletal proteins. Similarly, protein dynamics are also affected by mechanical stress which leads to accumulation of equatorial proteins during cytokinesis (Fig. 3.20).

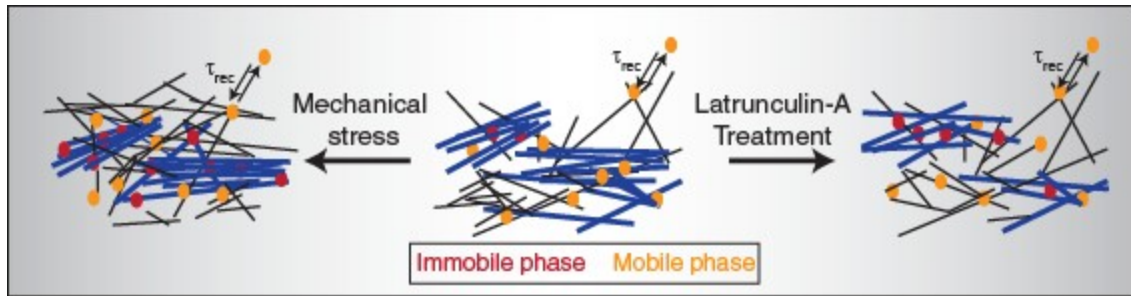


Figure 3.20: A schematic showing the changes in protein mobility arise from cytoskeletal rearrangement under mechanical stress or upon latrunculin-A treatment. Under high stress, the crosslinkers show reduced mobility leading to accumulation, while actin mobility increases even though filament amount is relatively unchanged. Upon latrunculin-A treatment, F-actin amount is reduced and actin mobility increases while the crosslinker mobility decreases significantly.

3.5. Proteomic analysis reveals interactions between myosin II, cortexillin I and IQGAP2

The cytokinesis and micropipette aspiration studies have demonstrated how the myosin II-cortexillin I mechanosensor and its regulation by IQGAPs is critical for cellular contractility and response to mechanical stresses [25]. The protein dynamics experiments emphasize the crosstalk between these stress-sensitive elements and their stabilization by mechanical stress. However, the molecular interactions potentiating the mechanosensory response remain unknown. Previous immunoprecipitation studies have shown that IQGAP1 and IQGAP2 interact with carboxy- and amino-terminal ends of cortexillin I respectively [34, 45, 46] (**Figure 3.21**). Since the cortexillin I-binding sites for both IQGAPs are distinct, stress-induced changes in IQGAP binding may result in the switching between a mechanosensitive and a non-mechanosensitive population of cortexillin I. However, it is likely that other protein-protein interactions might be important for regulating myosin II recruitment in the cleavage furrow and other sites of stress.

The localization of IQGAP2 and cortexillin I at the cleavage furrow is independent of many of the proteins known to be involved in mechanosensing. This hints towards the presence of unknown factors that govern protein recruitment. For example, cortexillin I has a PIP₂-binding domain [50] and could be directly or indirectly linked to the plasma membrane. IQGAP2 has also been shown to localize at membrane blebs [25], which are regions where the plasma membrane becomes detached from the cell cortex. Thus, the possibility of IQGAP2 binding to lipids or membrane proteins needs to be explored. The direct binding between myosin II and IQGAP1 or 2 is also a possible way by which these proteins affect mechanosensing. IQGAP has been shown to directly bind myosin tail in budding [51] and fission [52] yeast, and is required for myosin recruitment to the actin ring during cell division. In *Dictyostelium*, IQGAP2 also mediates a mechanotransduction pathway that feeds onto the mitotic spindle through the mitotic kinesin like protein Kif12. A previous study using mammalian cells has reported that a microtubule end-binding protein interacts with IQGAP1 and small GTPases to regulate cell polarity [53]. Similar associations could be important for the mechanosensory response of myosin II in *Dictyostelium*.

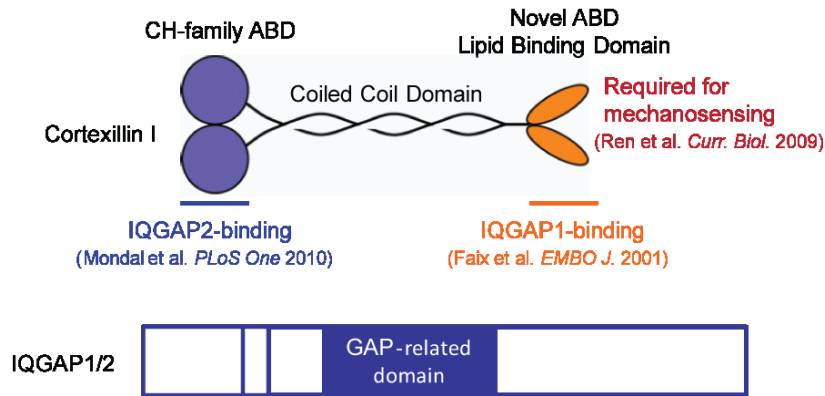


Figure 3.21: Domain organization of cortexillin I and IQGAP1/2. Cortexillin I has a calponin homology-family actin-binding domain (CH ABD), a coiled coil and a novel ABD and PIP₂-binding domain at the carboxyl-terminal tail (CT domain; orange). IQGAP2 is reported as binding to the CH domain, and IQGAP1 is reported as binding to the CT domain. The GAP-related domain (GRD) of the IQGAPs is thought to interact with Rac1-family proteins, cortexillin I and filamin.

Thus, we used a proteomic approach for the identification of binding partners for cortexillin I and IQGAP2. We expressed FLAG-tagged constructs of these proteins, and used immunoprecipitation to isolate the associated protein complexes. We used cytoskeletal fractionation to distinguish the protein complexes in the cytoskeleton versus those in the cytoplasm. Mass spectrometric analysis identified 12 and 46 cortexillin I-binding proteins in cytoskeletal and cytoplasmic samples respectively (**Table 5**). For IQGAP2, 12 and 14 proteins were found in the cytoskeletal and cytoplasmic samples respectively (**Table 6**). In addition to confirming the binding between cortexillin I and IQGAP2, we could also detect cortexillin I binding to Rac1, IQGAP1 and cortexillin II, as reported before [34, 45, 46, 54]. We did not detect any interaction between IQGAP2 and IQGAP1, supporting that these proteins likely bind different populations of cortexillin I, and thus have opposite effect on mechanosensing. Interestingly, both cortexillin I and IQGAP2 associate with myosin II, suggesting that these proteins could form a macromolecular complex that governs contractility. The experiments were conducted in the presence of Mg²⁺•ATP to prevent myosin II-binding to actin filaments.

Further, the myosin II-IQGAP2 interaction is also independent of cortexillin I, based on the proteomic analysis for samples from *ctxA/ctxB* cells expressing FLAG-GFP-IQGAP2 (**Table 7**). Interestingly, mass spectrometry also shows an interaction between RacE and myosin II (**Table 8**), which suggests that the polar cortex proteins could affect myosin II function through binding interactions consistent with 14-3-3-regulation of myosin II dynamics [16]. In addition to myosin II, many cytoskeletal and structural proteins having known roles in cytokinesis and contractility were also identified as binding partners for cortexillin I or IQGAP2 (**Fig. 3.22**). For example, *mmsdh* is found to associate with cortexillin I. Previously, *mmsdh* overexpression was shown to rescue the cleavage furrow localization of the assembly incompetent myosin mutant (3x Asp) [32]. This suggests that multiple parallel pathways are involved in cytokinesis regulation. Further characterization of these novel interactions will shed new light on how cells control their shape and division. We will use pair wise coimmunoprecipitation and two-color fluorescence cross-correlation spectroscopy to confirm and characterize these biochemical associations.

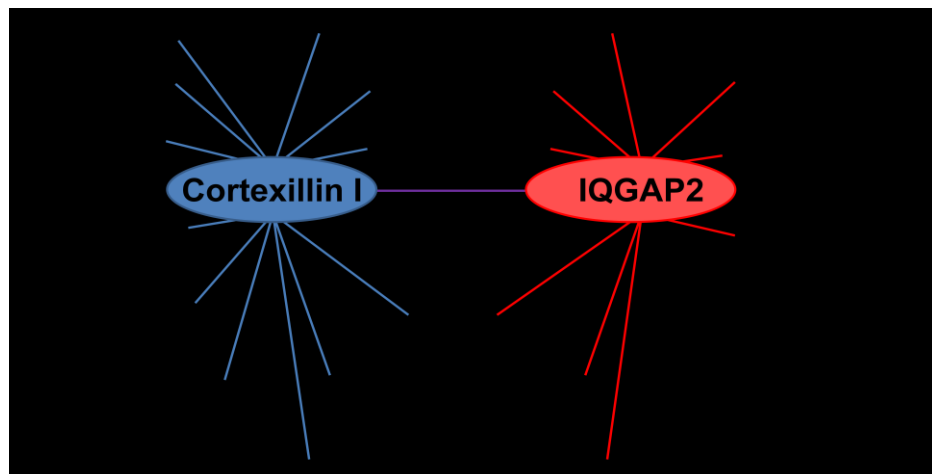


Figure 3.22: Selected potential proteins interacting with cortexillin I or IQGAP2, identified by proteomic analysis.

4. CONCLUSIONS

Mechanical stresses are important for driving cellular processes like cell division and motility, and play a major role in determining cell fate [25, 55, 56]. Understanding the effect of mechanical stress on protein dynamics is critical for having predictive power over these cellular behaviors. Here we identified that equatorial protein mobility significantly reduces at the cleavage furrow, while that of polar crosslinkers is unchanged. Both biochemical associations and myosin II-mediated remodeling affect protein dynamics. In addition to cleavage furrow contractility, compressive stress applied externally also leads to reduced protein mobility. Even when key contractile proteins are eliminated, the cytoskeleton is capable of maintaining fairly normal dynamics. Interestingly, most of the mutant phenotypes in protein dynamics are seen in the unstressed, interphase cortex, while the dynamics are unchanged across mutants during cytokinesis or upon compression. Thus, the cell's contractile system is built as a highly adaptive machine, maintaining fairly normal dynamics under mechanical stress ensuring fidelity of protein recruitment. In contrast, in other scenarios mechanical stress can exaggerate many mutant phenotypes. For example, *myoII* null cells cannot perform cytokinesis without substrate adhesion or when challenged by mechanical stress [8, 24]. Further, changes to cytoskeletal structure are sufficient to drive similar changes in protein dynamics, highlighting the importance of network properties in governing protein and cellular behaviors. Myosin II emerges as the major driver of active processes in the cortex, in accordance with previous studies [47].

The mechanical tuning of protein dynamics and recruitment is an important mode of regulating cellular responses to physical stimuli, and requires protein-protein interactions to be stabilized or disrupted under mechanical load. Protein-protein stabilization can induce protein clustering and provide signal amplification, while disruption can lead to signal dissipation. This is the classical paradigm for any signal transduction system. Basic molecular mechanisms for protein clustering in response to mechanical stress include catch bond formation and structural cooperativity, while slip bonds allow for force-induced disassembly. These fundamentals are important in directing macromolecular assembly of actin crosslinking proteins [5, 28, 57, 58]. Here we have demonstrated that these mechanisms are also applicable to scaffolding proteins like IQGAP2, emphasizing the importance of network structure and higher order self-assembly in governing cellular behavior. Indeed, cellular systems are engineered as smart materials where many of the constituents are mechanoresponsive.

Proteomic analysis shows that in addition to binding to each other, both cortexillin I and IQGAP2 also associate with myosin II. Further, the IQGAP2-myosin II interaction is independent of cortexillin I. These findings point towards the existence of macromolecular assemblies containing these proteins, which are responsive to mechanical stresses in the cortex. These biochemical interactions could also explain the mechanism by which all these proteins are stabilized at the furrow or under stress, as seen by the stress-dependent protein mobility shifts. The exact nature of these interactions is yet to be determined.

5. Future Work

5.1. Biochemical basis of mechanosensing

Numerous studies have characterized the effect of mechanical stresses on myosin II biochemistry. The myosin II-actin filament binding lifetime is stress-dependent. Further, upon binding to actin filament, myosin II induces conformational changes in the filament which promote cooperative binding of additional myosin II heads [5]. Myosin II also shows cooperative interactions with cortexillin I, which in turn promote the accumulation of these proteins in response to mechanical stress [5]. *In vivo* studies have shown that IQGAP proteins regulate cortexillin I accumulation and dynamics [25]. However, the exact nature of these interactions is unknown. A variety of cellular and biochemical assays can be used to study these molecular mechanisms in detail.

5.1.1. *In vivo* characterization of protein-protein interactions

The mass spectrometric analysis has identified potential interactions between myosin II-cortexillin I and IQGAP2. However, the relevance of these interactions in mechanosensing is uncharacterized. For example, certain protein complexes may only form when the cytoskeleton is under mechanical stress. To study *in vivo* formation of these protein complexes, we will use two-color fluorescence cross-correlation spectroscopy (FCCS). This will allow calculation of spatiotemporal changes in apparent binding coefficients for protein pairs under physiological conditions. Also, by studying these interactions in different genetic mutant backgrounds, we can analyze the additional factors that are important for the formation of these protein complexes. We will use

linked and unlinked GFP-mCherry fusions to calibrate the extent of binding. Due to technical limitations of *in vivo* FCCS which include low signal-to-noise ratio, poor control on protein expression and phototoxicity, we will also extend the analysis to cell lysates.

5.1.2. *In vitro* characterization of the myosin II, cortexillin I and IQGAP interactions

To achieve a molecular understanding of how IQGAPs regulate cortexillin I function, we can reduce the system to individual protein interactions. We have previously purified cortexillin I and myosin II [6, 16]. To express and purify the IQGAP proteins, we have designed and constructed a highly modular expression vector system based on the pBiEx series of vectors (Novagen). This system can be used for protein expression in either bacteria or insect cells, and contains cloning sites compatible with our *Dictyostelium* expression vectors. The vectors also contain a purification tag, carboxy- or amino-terminal fluorophores, and a TEV protease site to allow purification of labeled or unlabeled proteins from a single plasmid. Using this system, we have already expressed and partially purified IQGAP2.

We will confirm the *in vitro* binding of IQGAPs with cortexillin I using an analytical Superdex S200 10/30 size exclusion column. This column offers high resolution separation and Stokes radius measurement [59, 60], enabling us to differentiate protein complexes from individual proteins and test for competitive binding between the IQGAPs. Size exclusion also allows us to test for oligomerization of IQGAP1 and

IQGAP2, and the formation of higher order assemblies. Since cortexillin I is a known actin crosslinking and bundling protein [61-63], we will also determine whether IQGAPs affect cortexillin I-actin binding through *in vitro* co-sedimentation assays and negative staining electron microscopy. Additionally, we can also use quantitative assays such as fluorescence polarization anisotropy and isothermal titration calorimetry to measure the binding affinities for these proteins.

Myosin assembles into bipolar thick filaments (BTFs) in a salt-dependent manner. The ability to form these filaments is central to myosin II's force-bearing ability. One possible mode of regulating myosin II contractility could be the modulation of its filament forming ability by cortexillin I or IQGAP2. Thus, we will perform myosin II assembly assays with or without purified cortexillin I or IQGAP2. Collectively, these experiments will allow us to answer mechanistic questions about myosin II-cortexillin I-IQGAP complexes, and how they affect mechanosensing.

5.2.Reconstitution of contractile networks to determine the effect of mechanical stress on protein function and dynamics

After characterizing the myosin II-cortexillin I-IQGAP interactions *in vitro*, we will then test how the IQGAPs impact cortexillin I function using reconstituted actin networks. Reconstituted systems are uniquely poised for testing such mechanistic models, as they provide the desired level of complexity while eliminating the redundancies commonly found in biological systems. We have developed a custom-built uniaxial stretching device to apply force to actin networks (**Fig. 5.1**), which we can use to characterize the

effect of stress on IQGAP and cortexillin I function. We will measure the dynamics of cortexillin I under varying force to determine stress-dependence of actin-cortexillin I binding. By titrating in different amounts IQGAP2 and/or IQGAP1, we can examine how IQGAPs affect cortexillin I dynamics and whether they show competitive binding. By doing FRAP on the IQGAPs, we can test if there is a change in binding preference of cortexillin I for IQGAPs under mechanical stress. Further, we can test how cortexillin I affects the structure of stressed actin networks by imaging fluorescent actin filaments under TIRF, and if the IQGAPs regulate the crosslinking properties of cortexillin I. Collectively, these experiments will allow us to understand how IQGAPs regulate cortexillin I function during mechanosensing.

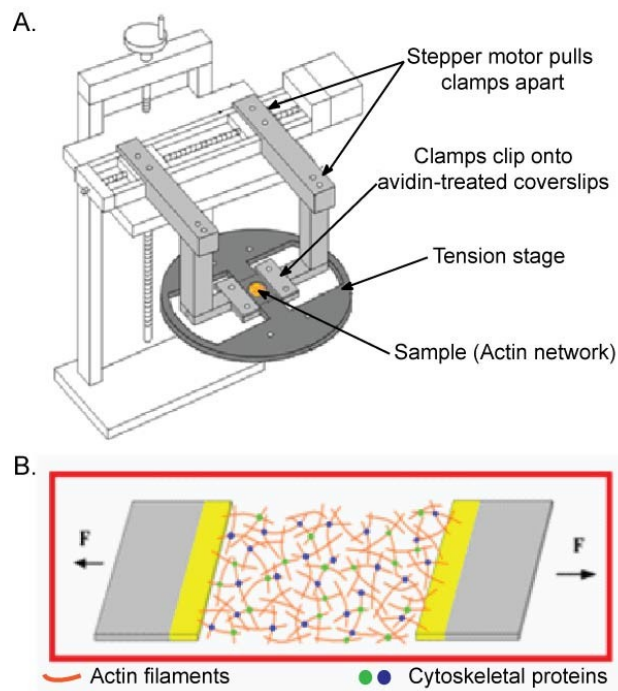


Figure 5.1: Device for imaging actin networks under stretch. **A.** Cartoon depicts the stretcher device. **B.** Assembled over a passivated imaging coverslip, the actin network includes biotin-labeled actin, which allows adhesion to the avidin-coated, stretching coverslips. The network can be controllably stretched while imaged by different modes (*e.g.* confocal, TIRF).

5.3. Mechanosensing regulation in dividing mammalian cells

We have developed a sophisticated understanding of the mechanosensory system in *Dictyostelium* that tunes contractility during cell division. The next step is to extend these studies to other systems, including mammalian cytokinesis. We have shown that myosin II is recruited to the aspiration site in interphase *Drosophila* S2 cells and HeLa cells (**Fig. 5.2**). We are also studying stress-dependent protein accumulation in mitotic HeLa cells using micropipette aspiration. To enhance the fraction of mitotic cells, we treated the cells with (+)S-Trityl-L-Cysteine (STLC) which results in metaphase arrest by forming a monopolar spindle [64]. Anaphase onset was induced using the Cdk1 inhibitor, Purvalanol [64]. We have shown that myosin IIA and IIB can accumulate at the aspiration site in both metaphase and anaphase cells, though the degree of accumulation varies through the cell cycle (**Fig. 5.3**).

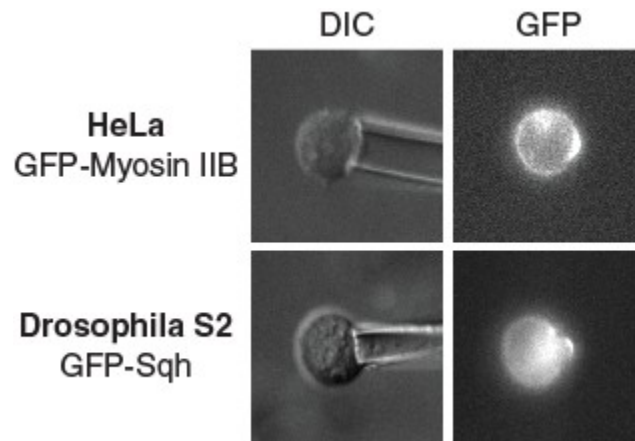


Figure 5.2: Myosin II accumulates upon micropipette aspiration in HeLa and S2 cells.

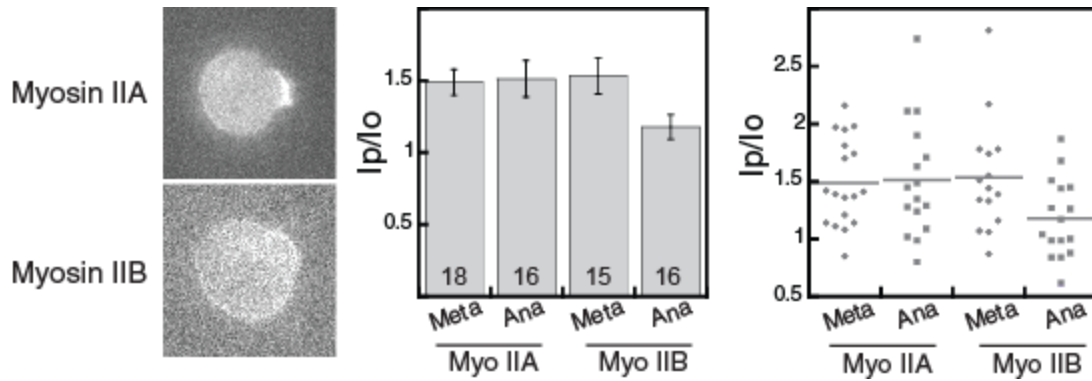


Figure 5.3: Myosin IIB is less responsive in anaphase HeLa cells.

We will next determine how other cleavage furrow proteins, such as anillin, MKLP1 and RhoA, respond to externally applied stress. We will also test if the application of mechanical stress affects the direction of spindle symmetry breaking during monopolar cytokinesis. Through these studies we will elucidate the pathways regulating mechanosensing and cytokinesis in mammalian cells.

Appendix

Table 1: Cell strains used in this study

Strain	Genotype	Experimental Applications
WT	Ax3(Rep orf+)	Phalloidin staining/F-actin quantification; MPA (cortical tension)
WT::GFP	Ax3(Rep orf+):Hyg ^R :pDRH; GFP, G418 ^R :pDM181	FRAP, FCS
WT::GFP	<i>myoII</i> (HS1)::mCH- <i>myoII</i> , Hyg ^R :pDRH; GFP, G418 ^R :pDM181	FRAP
WT::GFP-actin	KAx3(RF)::Hyg ^R :pDRH; GFP-actin, G418 ^R :pDM181	FRAP
WT::GFP-actin	<i>myoII</i> (HS1)::mCH- <i>myoII</i> , Hyg ^R :pDRH; GFP-actin, G418 ^R :pDM181	FRAP
WT::GFP-cortexillin I	KAX3(RF)::GFP-cortI, Hyg ^R :pDRH; G418 ^R :pDM181	FRAP, FCS
WT::GFP-IQGAP2	KAX3(RF)::RFP- α -tubulin, Hyg ^R :pDRH; GFP-IQGAP2, G418 ^R :pEXP4	FRAP, FCS
WT::FLAG-GFP	KAX3(RF):: Hyg ^R :pDRH; FLAG-GFP, G418 ^R :pDM181	Proteomics
<i>myoII</i> ::GFP-actin	<i>myoII</i> (HS1)::RFP- α -tubulin, Hyg ^R :pDRH; GFP-actin, G418 ^R :pDM181	FRAP
<i>myoII</i> ::GFP-cortexillin I	<i>myoII</i> (HS1)::GFP-cortI, Hyg ^R :pDRH; G418 ^R :pDM181	FRAP, FCS
<i>myoII</i> ::GFP-IQGAP2	<i>myoII</i> (HS1)::RFP- α -tubulin, Hyg ^R :pDRH; GFP-IQGAP2, G418 ^R :pEXP4	FRAP, FCS
<i>myoII</i> ::GFP	<i>myoII</i> (HS1)::Hyg ^R :pDRH; GFP, G418 ^R :pDM181	FRAP, FCS
S456L::GFP-cortexillin I	<i>myoII</i> (HS1)::GFP-cortI, Hyg ^R :pDRH; <i>myoII</i> (S456L), G418 ^R :pBIG	FRAP
S456L::GFP-IQGAP2	<i>myoII</i> (HS1)::CFP- <i>myoII</i> (S456L), Hyg ^R :pDRH; GFP-IQGAP2, G418 ^R :pEXP4	FRAP
<i>ctxA</i> ::GFP-actin	<i>cortI</i> (RF)::RFP- α -tubulin, Hyg ^R :pDRH; GFP-actin, G418 ^R :pDM181	FRAP
<i>ctxA</i> ::GFP-IQGAP2	<i>cortI</i> (RF)::RFP- α -tubulin, Hyg ^R :pDRH; GFP-IQGAP2, G418 ^R :pEXP4	FRAP, FCS
<i>ctxA</i> ::FLAG-GFP-cortexillin I	<i>cortI</i> (RF):: Hyg ^R :pDRH; FLAG-GFP-cort I, G418 ^R :pDM181	Proteomics

<i>ctxA/B</i> ::FLAG-GFP-IQGAP2	<i>cortI/II</i> (RF):: Hyg ^R :pDRH; FLAG-GFP-IQGAP2, G418 ^R :pDM181	Proteomics
<i>iqg2</i> ::GFP-actin	<i>iqgap2</i> (RF)::RFP- α -tubulin, Hyg ^R :pDRH; GFP-actin, G418 ^R :pDM181	FRAP
<i>iqg2</i> ::GFP-cortexillin I	<i>iqgap2</i> (RF)::GFP-cortI, Hyg ^R :pDRH; G418 ^R :pDM181	FRAP, FCS
<i>iqg2</i> ::FLAG-GFP-IQGAP2	<i>iqgap2</i> (RF):: Hyg ^R :pDRH; FLAG-GFP-IQGAP2, G418 ^R :pDM181	Proteomics
<i>iqg1</i> ::GFP-cortexillin I	<i>iqgap1</i> (RF)::GFP-cortI, Hyg ^R :pDRH; G418 ^R :pDM181	FRAP
<i>iqg1</i> ::GFP-IQGAP2	<i>iqgap1</i> (RF)::RFP- α -tubulin, Hyg ^R :pDRH; GFP-IQGAP2, G418 ^R :pEXP4	FRAP
<i>iqg1/2</i> ::GFP-cortexillin I	<i>Iqgap1/2</i> (RF)::GFP-cortI, Hyg ^R :pDRH; G418 ^R :pDM181	FRAP, FCS
<i>racE</i> ::GFP-actin	<i>racE</i> ^{24EH6} ::RFP- α -tubulin, Hyg ^R :pDRH; GFP-actin, G418 ^R :pDM181	FRAP
<i>racE</i> ::GFP-cortexillin I	<i>racE</i> ^{24EH6} ::GFP-cortI, Hyg ^R :pDRH; G418 ^R :pDM181	FRAP
<i>racE</i> ::GFP-IQGAP2	<i>racE</i> ^{24EH6} ::RFP- α -tubulin, Hyg ^R :pDRH; GFP-IQGAP2, G418 ^R :pEXP4	FRAP

Table 2: Mean recovery times (τ) and mean immobile fractions (F_i) for proteins in interphase cells, at the cleavage furrow and in compressed cells; FRAP Analysis

GFP-cortexillin I

	Interphase	Furrow	Compression
WT	2.1 ± 0.2 s, 0.14 ± 0.02 (23)	4.7 ± 0.6 s, 0.36 ± 0.04 (17)	2.9 ± 0.3 s, 0.46 ± 0.06 (14)
<i>myoII</i>	3.2 ± 0.5 s, 0.26 ± 0.04 (18)	4.1 ± 0.3 s, 0.43 ± 0.04 (23)	2.6 ± 0.5 s, 0.57 ± 0.06 (15)
<i>iqg2</i>	2.9 ± 0.2 s, 0.29 ± 0.05 (21)	3.6 ± 0.3 s, 0.36 ± 0.05 (23)	2.7 ± 0.3 s, 0.56 ± 0.03 (17)
<i>iqg1</i>	2.5 ± 0.3 s, 0.20 ± 0.04 (15)	5.8 ± 0.9 s, 0.44 ± 0.05 (15)	2.4 ± 0.3 s, 0.50 ± 0.05 (15)
<i>iqg1/2</i>	2.4 ± 0.2 s, 0.27 ± 0.04 (23)	2.7 ± 0.4 s, 0.56 ± 0.05 (17)	
<i>racE</i>	1.1 ± 0.2 s, 0.31 ± 0.07 (9)		
S456L	3.4 ± 0.4 s, 0.34 ± 0.03 (23)		

GFP-IQGAP2

	Interphase	Furrow	Compression
WT	1.6 ± 0.2 s, 0.10 ± 0.02 (14)	2.1 ± 0.2 s, 0.48 ± 0.04 (16)	1.7 ± 0.1 s, 0.27 ± 0.04 (20)
<i>myoII</i>	1.6 ± 0.2 s, 0.30 ± 0.04 (18)	3.3 ± 0.3 s, 0.48 ± 0.05 (15)	2.7 ± 0.5 s, 0.64 ± 0.04 (15)
<i>ctxA</i>	1.5 ± 0.2 s, 0.06 ± 0.02 (13)	2.0 ± 0.3 s, 0.36 ± 0.04 (13)	2.1 ± 0.2 s, 0.30 ± 0.02 (14)
<i>iqg1</i>	1.5 ± 0.3 s, 0.16 ± 0.03 (18)	2.7 ± 0.3 s, 0.43 ± 0.04 (17)	2.3 ± 0.3 s, 0.33 ± 0.04 (16)
<i>racE</i>	1.4 ± 0.4 s, 0.17 ± 0.04 (16)		
S456L	1.8 ± 0.2 s, 0.22 ± 0.04 (13)		

GFP-actin

	Interphase	Furrow	Compression
WT	0.75 ± 0.15 s, 0.39 ± 0.05 (17)	1.3 ± 0.2 s, 0.28 ± 0.04 (17)	0.70 ± 0.06 s, 0.29 ± 0.01 (14)
<i>myoII</i>	0.68 ± 0.12 s, 0.43 ± 0.05 (11)		
<i>ctxA</i>	0.61 ± 0.12 s, 0.35 ± 0.05 (10)		
<i>iqg2</i>	0.46 ± 0.03 s, 0.34 ± 0.05 (15)		
<i>racE</i>	0.61 ± 0.18 s, 0.25 ± 0.07 (10)		

GFP

	Interphase	Furrow	Compression
WT	0.26 ± 0.03 s, 0.12 ± 0.02 (27)	0.27 ± 0.07 s, 0.12 ± 0.03 (12)	0.66 ± 0.12 s, 0.26 ± 0.04 (14)
<i>myoII</i>	0.35 ± 0.03 s, 0.14 ± 0.03 (15)		0.50 ± 0.06 s, 0.11 ± 0.02 (15)

The values represent mean ± SEM for recovery times and immobile fractions. The number of measurements is given in parentheses.

Table 3: Mean recovery times (τ) and mean immobile fractions (F_i) for proteins latrunculin-A or jasplakinolide treated cells; FRAP Analysis

	DMSO		5 μM Latrunculin-A		2 μM Jasplakinolide	
GFP cortI (interphase)	2.5 \pm 0.4 s,	0.25 \pm 0.04 (14)	3.5 \pm 0.6 s,	0.53 \pm 0.05 (13)	2.2 \pm 0.4 s,	0.46 \pm 0.06 (15)
GFP cortI (furrow)	4.6 \pm 0.8 s,	0.53 \pm 0.10 (9)	6.2 \pm 1.1 s,	0.60 \pm 0.04 (16)		
GFP IQGAP2	1.5 \pm 0.2 s,	0.19 \pm 0.03 (14)	2.0 \pm 0.2 s,	0.26 \pm 0.03 (19)	1.1 \pm 0.1 s,	0.14 \pm 0.02 (23)
GFP actin	0.66 \pm 0.05 s,	0.36 \pm 0.02 (68)	1.1 \pm 0.13 s,	0.25 \pm 0.03 (41)	0.82 \pm 0.08 s,	0.44 \pm 0.03 (22)
GFP	0.26 \pm 0.03 s,	0.12 \pm 0.02 (27)	0.40 \pm 0.03 s,	0.20 \pm 0.02 (15)	0.39 \pm 0.03 s,	0.10 \pm 0.02 (15)

The values represent mean \pm SEM for recovery times and immobile fractions. The number of measurements is given in parentheses.

Table 4: Cytosolic diffusion times (τ_D) and diffusion coefficients (D_{eff}) for proteins as measured by FCS

Diffusion in PBS at 22°C

	Molecular weight (kDa)	Diffusion time (τ_D)	Diffusion Coefficient (D_{eff})
Rhodamine 6G	0.48 kDa	0.033 ± 0.002 ms (34)	426 $\mu\text{m}^2/\text{s}^*$
His-mCherry	28 kDa	0.15 ± 0.01 ms (11)	94 $\mu\text{m}^2/\text{s}$ (Reported value: 95 $\mu\text{m}^2/\text{s}^*$)
His-GFP-cortexillin-I	80 kDa	0.28 ± 0.02 ms (11)	50.2 $\mu\text{m}^2/\text{s}$

Diffusion in cytoplasm at 22°C

Cell line	Cortexillin I	IQGAP2	GFP
WT control	2.4 ± 0.2 ms (20), $D_{eff} = 5.8 \mu\text{m}^2/\text{s}$	2.9 ± 0.3 ms (18), $D_{eff} = 4.8 \mu\text{m}^2/\text{s}$	0.78 ± 0.05 ms (20), $D_{eff} = 18 \mu\text{m}^2/\text{s}$
WT + compression	4.0 ± 0.3 ms (17), $D_{eff} = 3.5 \mu\text{m}^2/\text{s}$	3.4 ± 0.4 ms (16), $D_{eff} = 4.1 \mu\text{m}^2/\text{s}$	1.5 ± 0.1 ms (16), $D_{eff} = 9.4 \mu\text{m}^2/\text{s}$
<i>myoII</i>	2.6 ± 0.2 ms (18), $D_{eff} = 5.4 \mu\text{m}^2/\text{s}$	2.9 ± 0.2 ms (11), $D_{eff} = 4.8 \mu\text{m}^2/\text{s}$	1.4 ± 0.2 ms (15), $D_{eff} = 10 \mu\text{m}^2/\text{s}$
<i>myoII</i> + compression	3.9 ± 0.4 ms (12), $D_{eff} = 3.6 \mu\text{m}^2/\text{s}$	-	0.69 ± 0.06 ms (14), $D_{eff} = 20 \mu\text{m}^2/\text{s}$
<i>iqg2</i>	3.1 ± 0.2 ms (16), $D_{eff} = 4.5 \mu\text{m}^2/\text{s}$	-	-
<i>iqg1/2</i>	3.7 ± 0.3 ms (16), $D_{eff} = 3.8 \mu\text{m}^2/\text{s}$	-	-
<i>ctxA</i>	-	2.6 ± 0.3 ms (12), $D_{eff} = 5.4 \mu\text{m}^2/\text{s}$	-

Treatment	Cortexillin I	IQGAP2	GFP
DMSO	2.8 ± 0.4 ms (12), $D_{eff} = 5.0 \mu\text{m}^2/\text{s}$	2.7 ± 0.4 ms (15), $D_{eff} = 5.2 \mu\text{m}^2/\text{s}$	0.75 ± 0.10 ms (13), $D_{eff} = 19 \mu\text{m}^2/\text{s}$
5 μM latrunculin-A	P1: 2.4 ± 0.1 ms (8), $D_{eff} = 5.8 \mu\text{m}^2/\text{s}$ P2: 8.1 ± 0.5 ms (7), $D_{eff} = 1.7 \mu\text{m}^2/\text{s}$	3.6 ± 0.4 ms (16), $D_{eff} = 3.9 \mu\text{m}^2/\text{s}$	1.1 ± 0.1 ms (25), $D_{eff} = 13 \mu\text{m}^2/\text{s}$
2 μM jasplakinolide	3.2 ± 0.2 ms (20), $D_{eff} = 4.4 \mu\text{m}^2/\text{s}$	3.2 ± 0.4 ms (18), $D_{eff} = 4.4 \mu\text{m}^2/\text{s}$	0.86 ± 0.07 ms (18), $D_{eff} = 16 \mu\text{m}^2/\text{s}$

The values represent mean ± SEM for diffusion times. The numbers of measurements is given in parentheses.

* Diffusion coefficients for rhodamine 6G and GFP were reported in Petrášek and Schwille (2008) [37].

Table 5: List of potential cortexillin I-binding proteins

Gene Name	Protein Name	Control	Cort I	G-value
Cytoskeletal fraction				
ctxA	Cortexillin-1	0.0	16.5	22.8
rgaA	IQGAP1	0.0	16.4	22.7
ctxB	Cortexillin-2	0.0	13.4	18.5
mhcA	Myosin-2 heavy chain	2.3	12.1	7.3
mfap1	Protein MFAP1 homolog	0.0	4.9	6.8
gapA	IQGAP2	0.0	4.9	6.8
DDB_0218327	Putative uncharacterized protein	0.0	3.7	5.1
DDB_0186471	RNA-binding region RNP-1 domain-containing protein	0.0	3.4	4.8
efbA	Elongation factor 2	0.0	3.3	4.6
rac1A	Rho-related protein rac1A	0.0	3.3	4.6
ndufa12	NADH dehydrogenase[ubiquinone]1 alpha subcomplex subunit 12	0.0	3.0	4.1
patB	Probable plasma membrane ATPase	0.0	2.9	4.1
mleE	Myosin essential light chain	0.0	2.6	3.6
Cytoplasmic fraction				
act22	Putative actin-22	0.0	32.2	44.6
DICPUDRAFT_90232	Putative uncharacterized protein	0.0	29.1	40.3
rgaA	IQGAP1	0.0	25.6	35.5
mhcA	Myosin-2 heavy chain	2.0	31.8	31.5
ctxA	Cortexillin-1	0.0	22.3	30.9
fkbp5	FK506-binding protein 5	0.0	14.8	20.6
ctxB	Cortexillin-2	0.0	14.6	20.2
cdcD	Cell division cycle protein 48	26.3	65.5	17.3
gapA	IQGAP2	0.0	11.5	16.0
ctr9	RNA polymerase II complex component	0.0	9.6	13.4
pyr1-3	Protein PYR1-3	0.0	8.0	11.1
efbA	Elongation factor 2	0.0	6.7	9.3
DICPUDRAFT_93127	Putative uncharacterized protein	0.0	6.7	9.3
DDB_0188474	DUF814 family protein	0.0	6.1	8.4
eef1a1	Elongation factor 1-alpha	3.9	16.1	7.9
rps3a	40S ribosomal protein S3	1.4	10.3	7.6
DDB_G0291301	Putative bifunctional amineoxidase	0.0	5.5	7.6
leo1	RNA polymerase-associated protein	0.0	5.4	7.5

acpB	F-actin-capping protein subunit alpha	0.0	5.3	7.4
paf1	RNA polymerase II-associated factor 1	0.0	5.0	6.9
ifdA	DEAD/DEAH box helicase domain-containing protein	0.0	4.9	6.7
tufm	Elongation factor Tu, mitochondrial	0.0	4.8	6.6
DDB_G0282483	Uncharacterized transmembrane protein	0.0	4.4	6.1
cdc73	RNA polymerase II complex component	0.0	4.1	5.7
acly	Probable ATP-citrate synthase	0.0	4.0	5.5
DDB_0169491	Putative uncharacterized protein	0.0	4.0	5.5
rpl13	60S ribosomal protein L13	0.0	3.8	5.3
DD8-14	AAA ATPase domain-containing protein	0.0	3.8	5.2
metK	S-adenosyl methionine synthase	0.0	3.7	5.2
rps23	40S ribosomal protein S23	0.0	3.5	4.9
DDB_G0277077	UvrB/UvrC domain-containing protein	0.0	3.5	4.9
DDB_0187217	Putative uncharacterized protein	0.0	3.4	4.7
mcfQ	Mitochondrial substrate carrier family protein Q	0.0	3.3	4.6
DICPUDRAFT_52099	40S ribosomal protein S26	0.0	3.2	4.5
abpC	Gelation factor	0.0	3.2	4.4
tubB	Tubulin beta-chain	0.0	3.1	4.3
rpl30	60S ribosomal protein L30	3.2	10.7	4.3
mmsdh	Probable methylmalonate-semialdehyde dehydrogenase[acylating], mitochondrial	0.0	3.1	4.2
wdr61	WD repeat-containing protein61	0.0	3.1	4.2
cyc1	Cytochrome c1, heme protein, mitochondrial	0.0	3.1	4.2
mcfZ	Mitochondrial substrate carrier family protein Z	0.0	3.0	4.1
rpl18	60S ribosomal protein L18	0.0	3.0	4.1
pdhC	Dihydrolipoyllysine-residue acetyltransferase component of pyruvate dehydrogenase complex, mitochondrial	0.0	2.8	3.9
DICPUDRAFT_48405	Putative uncharacterized protein	0.0	2.7	3.7
rac1A	Rho-related protein rac1A	0.0	2.7	3.7
odhB	Dihydrolipoyllysine-residue succinyltransferase component of 2-oxoglutarate dehydrogenase complex, mitochondrial	0.0	2.7	3.7
mleE	Myosin essential light chain	0.0	2.7	3.7

Table 6: List of potential IQGAP2-binding proteins

Gene Name	Protein Name	Control	IQGAP2	G-value
Cytoskeletal fraction				
act1	Major actin	0.0	27.3	37.91
hspA	60kDa heat shock protein, mitochondrial	4.7	24.1	14.40
gapA	IQGAP2	0.0	9.8	13.54
act24	Putative actin-24	0.0	8.8	12.19
dscA	Discoidin-1 subunit A	0.0	6.2	8.60
ctxB	Cortexillin-2	0.0	6.1	8.41
ctxA	Cortexillin-1	0.0	5.1	7.08
act18	Actin-18	0.0	4.8	6.66
DDB_0218327	Putative uncharacterized protein	0.0	4.4	6.16
rpl12	60S ribosomal protein L12	0.0	4.4	6.07
mleE	Myosin essential light chain	0.0	3.5	4.81
rplp2	60S acidic ribosomal protein P2	7.9	17.8	3.94
efbA	Elongation factor 2	0.0	2.8	3.91
Cytoplasmic fraction				
dscA	Discoidin-1 subunit A	0.0	17.0	23.60
mhcA	Myosin-2 heavy chain	2.0	19.3	16.14
gapA	IQGAP2	0.0	9.9	13.66
ctxB	Cortexillin-2	0.0	8.0	11.07
ctxA	Cortexillin-1	0.0	7.6	10.49
dscC	Discoidin-1 subunitB/C	7.2	24.8	10.31
fkbp5	FK506-binding protein 5	0.0	7.3	10.18
leo1	RNA polymerase-associated protein	0.0	6.4	8.85
rplp2	60S acidic ribosomal protein P2	8.3	22.0	6.45
dscE	Discoidin-2	4.6	15.6	6.38
cadA	Calcium-dependent cell adhesion molecule	0.0	4.0	5.55
rplp1	60S acidic ribosomal protein P1	1.4	8.1	5.27
cdcD	Cell division cycle protein 48	26.3	43.6	4.32
acpB	F-actin-capping protein subunit alpha	0.0	3.0	4.19
DICPUDRAFT_74418	Putative uncharacterized protein	0.0	2.9	4.01

Table 7: List of potential IQGAP2-binding proteins in *ctxA/B* null cells

Gene Name	Protein Name	Control	IQGAP2	G-value
Cytoskeletal fraction				
act18	Actin-18	0.0	3.3	4.61
gapA	IQGAP2	0.0	2.6	3.66
Cytoplasmic fraction				
mhcA	Myosin-2 heavy chain	2.0	66.1	76.13
fkbp5	FK506-binding protein 5	0.0	11.0	15.27
leo1	RNA polymerase-associated protein	0.0	5.7	7.84
acpB	F-actin-capping protein subunit alpha	0.0	5.4	7.55
cdcD	Cell division cycle protein 48	26.3	49.2	7.07
ctr9	RNA polymerase II complex component	0.0	4.6	6.40
mlcE	Myosin essential light chain	0.0	4.3	6.00
gapA	IQGAP2	0.0	4.3	5.95
mcfZ	Mitochondrial substrate carrier family protein Z	0.0	3.0	4.12

Table 8: List of potential RacE-binding proteins

Gene Name	Protein Name	Control	RacE	G-value
Cytoskeletal fraction				
mppA2	Mitochondrial-processing peptidase subunit alpha-2	2.2	19.4	15.80
racE	Rho-related protein racE	0.0	9.3	12.85
efbA	Elongation factor 2	0.0	8.0	11.08
atp5b	ATP synthase subunit beta, mitochondrial	4.0	18.9	10.64
mppB	Mitochondrial-processing peptidase subunit beta	0.0	6.6	9.09
atp5C1	ATP synthase subunit gamma, mitochondrial	0.0	6.1	8.41
DICPUDRAFT_52984	ATP synthase subunit beta	0.0	5.6	7.81
if1	F1F0-ATPase putative regulatory protein IF1	0.0	5.1	7.01
rpl12	60S ribosomal protein L12	0.0	4.8	6.61
atp5O	ATP synthase subunit O, mitochondrial	0.0	4.6	6.39
acly	Probable ATP-citrate synthase	0.0	4.5	6.22
arcE	Actin-related protein2/3 complex subunit 5	0.0	4.4	6.09
ndufa12	NADH dehydrogenase[ubiquinone]1 alpha subcomplex subunit 12	0.0	4.4	6.06
DDB_0167260	Putative uncharacterized protein	0.0	4.4	6.03
smt1	Probable cycloartenol-C-24-methyltransferase 1	0.0	4.3	5.99
DDB_0185950	Putative uncharacterized protein	7.3	19.8	5.98
leo1	RNA polymerase-associated protein	0.0	4.2	5.79
acpB	F-actin-capping protein subunit alpha	0.8	6.3	4.95
cyc1	Cytochrome c1, hemeprotein, mitochondrial	0.0	3.5	4.89
DDB_G0283843	Uncharacterized protein	0.8	6.2	4.87
atp1	ATP synthase subunit alpha, mitochondrial	0.9	6.7	4.86
sdhA	Succinate dehydrogenase[ubiquinone] flavoprotein subunit, mitochondrial	0.0	3.2	4.47
pks16	Probable polyketide synthase 16	0.0	3.2	4.39
mecr	Trans-2-enoyl-CoA reductase, mitochondrial	0.0	3.1	4.36
DDB_0169073	Putative uncharacterized protein	0.0	3.1	4.29
DDB_0205386	Putative uncharacterized protein	0.0	3.1	4.29
sdhB	Succinate dehydrogenase[ubiquinone] iron-sulfur subunit, mitochondrial	0.0	3.0	4.19
DDB_0186283	Putative uncharacterized protein	0.0	3.0	4.17
DDB_0191803	Putative uncharacterized protein	0.0	3.0	4.17
mlcE	Myosin essential light chain	0.0	3.0	4.16

DDB_0186471	RNA-binding region RNP-1 domain-containing protein	0.0	3.0	4.14
cmfB	Conditioned medium factor receptor 1	0.0	2.9	4.07
act18	Actin-18	0.0	2.8	3.94
rps23	40S ribosomal protein S23	0.0	2.8	3.84
rpl13	60S ribosomal protein L13	0.0	2.8	3.84
ddj1	Heat shock protein	0.0	2.8	3.84
DDB_G0282483	Uncharacterized transmembrane protein	0.0	2.8	3.84
cdcD	Cell division cycle protein 48	16.3	29.4	3.84
tubB	Tubulin beta chain	0.0	2.3	3.22
Cytoplasmic fraction				
mhcA	Myosin-2 heavy chain	2.0	74.9	87.89
act22	Putative actin-22	0.0	37.9	52.55
racE	Rho-related protein racE	0.0	5.7	7.95
leo1	RNA polymerase-associated protein	0.0	5.4	7.46
dscA	Discoidin-1 subunit A	0.0	4.7	6.57
mlcR	Myosin regulatory light chain	0.0	4.6	6.44
fkbp5	FK506-binding protein 5	0.0	4.0	5.50
cdcD	Cell division cycle protein 48	26.3	44.7	4.81
mlcE	Myosin essential light chain	0.0	3.2	4.48
acpB	F-actin-capping protein subunit alpha	0.0	2.8	3.84

Contributions

I would like to thank the following co-authors for their contributions to this study: Irina Tchernyshyov, Jennifer van Eyk, Eric R. Griffis and Douglas N. Robinson. I.T. performed the mass spectrometric analysis; J.V.E. supervised I.T. on the proteomics work. V.S. and E.R.G. conducted the experiments on mitotic HeLa cells. V.S. conducted all the experiments. V.S. and D.N.R. designed the experiments, analyzed the data, and prepared the manuscript. D.N.R. supervised the projects.

Part of this work has been submitted to *Current Biology* for publication as: Srivastava V. and Robinson D.N. “Mechanical stress and network structure drive protein dynamics during cytokinesis.” *Current Biology* **25**(5): 663-670. Current Biology gives authors rights to include the article in full or in part in a thesis or dissertation (provided that this is not to be published commercially).

Bibliography

1. Canman, J.C., and Wells, W.A. (2004). Rappaport Furrows on Our Minds: The ASCB Cytokinesis Meeting Burlington, VT July 22–25, 2004. *The Journal of Cell Biology* *166*, 943-948.
2. Eggert, U.S., Mitchison, T.J., and Field, C.M. (2006). Animal Cytokinesis: From Parts List to Mechanisms. *Annual Review of Biochemistry* *75*, 543-566.
3. Robinson, D.N., Kee, Y.S., Luo, T., and Surcel, A. (2012). 7.5 Understanding How Dividing Cells Change Shape. In *Comprehensive Biophysics*, E.H. Egelman, ed. (Amsterdam: Elsevier), pp. 48-72.
4. West-Foyle, H., and Robinson, D.N. (2012). Cytokinesis mechanics and mechanosensing. Cytoskeleton, n/a-n/a.
5. Luo, T., Mohan, K., Srivastava, V., Ren, Y., Iglesias, P.A., and Robinson, D.N. (2012). Understanding the Cooperative Interaction between Myosin II and Actin Cross-Linkers Mediated by Actin Filaments during Mechanosensation. *Biophysical Journal* *102*, 238-247.
6. Ren, Y., Effler, J.C., Norstrom, M., Luo, T., Firtel, R.A., Iglesias, P.A., Rock, R.S., and Robinson, D.N. (2009). Mechanosensing through Cooperative Interactions between Myosin II and the Actin Crosslinker Cortexillin I. *19*, 1421-1428.
7. Egelhoff, T.T., Lee, R.J., and Spudich, J.A. (1993). Dictyostelium myosin heavy chain phosphorylation sites regulate myosin filament assembly and localization in vivo. *Cell* *75*, 363-371.
8. Lozanne, A.D., and Spudich, J.A. (1987). Disruption of the Dictyostelium Myosin Heavy Chain Gene by Homologous Recombination. *Science* *236*, 1086-1091.
9. Poirier, C.C., Ng, W.P., Robinson, D.N., and Iglesias, P.A. (2012). Deconvolution of the Cellular Force-Generating Subsystems that Govern Cytokinesis Furrow Ingression. *PLoS Comput Biol* *8*, e1002467.
10. Piekny, A.J., and Glotzer, M. (2008). Anillin Is a Scaffold Protein That Links RhoA, Actin, and Myosin during Cytokinesis. *Current Biology* *18*, 30-36.
11. Weber, I., Gerisch, G., Heizer, C., Murphy, J., Badelt, K., Stock, A., Schwartz, J.-M., and Faix, J. (1999). Cytokinesis mediated through the recruitment of cortexillins into the cleavage furrow. *EMBO J* *18*, 586-594.
12. Jaffe, A.B., and Hall, A. (2005). RHO GTPASES: Biochemistry and Biology. *Annual Review of Cell and Developmental Biology* *21*, 247-269.
13. Piekny, A., Werner, M., and Glotzer, M. (2005). Cytokinesis: welcome to the Rho zone. *Trends in Cell Biology* *15*, 651-658.
14. Glotzer, M. (2005). The Molecular Requirements for Cytokinesis. *Science* *307*, 1735-1739.
15. Foe, V.E., and von Dassow, G. (2008). Stable and dynamic microtubules coordinately shape the myosin activation zone during cytokinetic furrow formation. *The Journal of Cell Biology* *183*, 457-470.
16. Zhou, Q., Kee, Y.-S., Poirier, C.C., Jelinek, C., Osborne, J., Divi, S., Surcel, A., Will, M.E., Eggert, U.S., Müller-Taubenberger, A., et al. (2010). 14-3-3

- Coordinates Microtubules, Rac, and Myosin II to Control Cell Mechanics and Cytokinesis. *Current Biology* *20*, 1881-1889.
17. Robinson, D., Cavet, G., Warrick, H., and Spudich, J. (2002). Quantitation of the distribution and flux of myosin-II during cytokinesis. *BMC Cell Biology* *3*, 1-13.
 18. Echard, A. (2012). Phosphoinositides and cytokinesis: The “PIP” of the iceberg. *Cytoskeleton* *69*, 893-912.
 19. Field, S.J., Madson, N., Kerr, M.L., Galbraith, K.A.A., Kennedy, C.E., Tahiliani, M., Wilkins, A., and Cantley, L.C. (2005). PtdIns(4,5)P₂ Functions at the Cleavage Furrow during Cytokinesis. *15*, 1407-1412.
 20. Reichl, E.M., Effler, J.C., and Robinson, D.N. (2005). The stress and strain of cytokinesis. *Trends in Cell Biology* *15*, 200-206.
 21. Zhang, W., and Robinson, D.N. (2005). Balance of actively generated contractile and resistive forces controls cytokinesis dynamics. *Proceedings of the National Academy of Sciences of the United States of America* *102*, 7186-7191.
 22. Luo, T., Srivastava, V., Ren, Y., and Robinson, D.N. (2014). Mimicking the mechanical properties of the cell cortex by the self-assembly of an actin cortex in vesicles. *Applied Physics Letters* *104*, -.
 23. Hochmuth, R.M. (2000). Micropipette aspiration of living cells. *Journal of Biomechanics* *33*, 15-22.
 24. Effler, J.C., Kee, Y.-S., Berk, J.M., Tran, M.N., Iglesias, P.A., and Robinson, D.N. (2006). Mitosis-Specific Mechanosensing and Contractile-Protein Redistribution Control Cell Shape. *Current Biology* *16*, 1962-1967.
 25. Kee, Y.-S., Ren, Y., Dorfman, D., Iijima, M., Firtel, R., Iglesias, P.A., and Robinson, D.N. (2012). A mechanosensory system governs myosin II accumulation in dividing cells. *Molecular Biology of the Cell* *23*, 1510-1523.
 26. Girard, K.D., Chaney, C., Delannoy, M., Kuo, S.C., and Robinson, D.N. (2004). Dynacortin contributes to cortical viscoelasticity and helps define the shape changes of cytokinesis. *EMBO J* *23*, 1536-1546.
 27. Reichl, E.M., Ren, Y., Morphew, M.K., Delannoy, M., Effler, J.C., Girard, K.D., Divi, S., Iglesias, P.A., Kuo, S.C., and Robinson, D.N. (2008). Interactions between Myosin and Actin Crosslinkers Control Cytokinesis Contractility Dynamics and Mechanics. *18*, 471-480.
 28. Luo, T., Mohan, K., Iglesias, P.A., and Robinson, D.N. (2013). Molecular mechanisms of cellular mechanosensing. *Nat Mater* *12*, 1064-1071.
 29. Gerald, N., Dai, J., Ting-Beall, H.P., and De Lozanne, A. (1998). A Role for Dictyostelium RacE in Cortical Tension and Cleavage Furrow Progression. *J. Cell Biol.* *141*, 483-492.
 30. Robinson, D.N., and Spudich, J.A. (2000). Dynacortin, a Genetic Link between Equatorial Contractility and Global Shape Control Discovered by Library Complementation of a Dictyostelium discoideum Cytokinesis Mutant. *J. Cell Biol.* *150*, 823-838.
 31. Zang, J.-H., and Spudich, J.A. (1998). Myosin II localization during cytokinesis occurs by a mechanism that does not require its motor domain. *Proceedings of the National Academy of Sciences* *95*, 13652-13657.
 32. Ren, Y., West-Foyle, H., Surcel, A., Miller, C., and Robinson, D.N. (2014). Genetic suppression of a phosphomimic myosin II identifies system-level factors

- that promote myosin II cleavage furrow accumulation. *Molecular Biology of the Cell* 25, 4150-4165.
33. Ruppel, K.M., Uyeda, T.Q., and Spudich, J.A. (1994). Role of highly conserved lysine 130 of myosin motor domain. In vivo and in vitro characterization of site specifically mutated myosin. *Journal of Biological Chemistry* 269, 18773-18780.
 34. Lee, S., Shen, Z., Robinson, D.N., Briggs, S., and Firtel, R.A. (2010). Involvement of the Cytoskeleton in Controlling Leading-Edge Function during Chemotaxis. *Molecular Biology of the Cell* 21, 1810-1824.
 35. Fukui, Y., Yumura, S., Yumura, T.K., and Mori, H. (1986). Agar overlay method: high-resolution immunofluorescence for the study of the contractile apparatus. *Methods Enzymol* 134, 573-580.
 36. Fukui, Y., Yumura, S., and Yumura, T.K. (1987). Agar-overlay immunofluorescence: high-resolution studies of cytoskeletal components and their changes during chemotaxis. *Methods Cell Biol* 28, 347-356.
 37. Petrášek, Z., and Schwille, P. Precise Measurement of Diffusion Coefficients using Scanning Fluorescence Correlation Spectroscopy. *Biophysical Journal* 94, 1437-1448.
 38. Reines, D., and Clarke, M. (1985). Immunochemical analysis of the supramolecular structure of myosin in contractile cytoskeletons of Dictyostelium amoebae. *Journal of Biological Chemistry* 260, 14248-14254.
 39. Haugwitz, M., Noegel, A.A., Karakesisoglou, J., and Schleicher, M. (1994). Dictyostelium amoebae that lack G-actin-sequestering profilins show defects in F-actin content, cytokinesis, and development. *Cell* 79, 303-314.
 40. Uehara, R., Goshima, G., Mabuchi, I., Vale, R.D., Spudich, J.A., and Griffis, E.R. (2010). Determinants of Myosin II Cortical Localization during Cytokinesis. *Current Biology* 20, 1080-1085.
 41. Yumura, S. (2001). Myosin II dynamics and cortical flow during contractile ring formation in Dictyostelium cells. *The Journal of Cell Biology* 154, 137-146.
 42. Murphy, C.T., Rock, R.S., and Spudich, J.A. (2001). A myosin II mutation uncouples ATPase activity from motility and shortens step size. *Nat Cell Biol* 3, 311-315.
 43. Guha, M., Zhou, M., and Wang, Y.-l. (2005). Cortical Actin Turnover during Cytokinesis Requires Myosin II. *Current Biology* 15, 732-736.
 44. Murthy, K., and Wadsworth, P. (2005). Myosin-II-Dependent Localization and Dynamics of F-Actin during Cytokinesis. *Current Biology* 15, 724-731.
 45. Faix, J., Weber, I., Mintert, U., Kohler, J., Lottspeich, F., and Marriott, G. (2001). Recruitment of cortexillin into the cleavage furrow is controlled by Rac1 and IQGAP-related proteins. *EMBO J* 20, 3705-3715.
 46. Mondal, S., Burgute, B., Rieger, D., Müller, R., Rivero, F., Faix, J., Schleicher, M., and Noegel, A.A. (2010). Regulation of the Actin Cytoskeleton by an Interaction of IQGAP Related Protein GAPA with Filamin and Cortexillin I. *PLoS ONE* 5, e15440.
 47. Girard, K.D., Kuo, S.C., and Robinson, D.N. (2006). Dictyostelium myosin II mechanochemistry promotes active behavior of the cortex on long time scales. *Proceedings of the National Academy of Sciences of the United States of America* 103, 2103-2108.

48. Faix, J., Steinmetz, M., Boves, H., Kammerer, R.A., Lottspeich, F., Mintert, U., Murphy, J., Stock, A., Aebi, U., and Gerisch, G. (1996). Cortexillins, Major Determinants of Cell Shape and Size, Are Actin-Bundling Proteins with a Parallel Coiled-Coil Tail. *Cell* *86*, 631-642.
49. Robinson, D.N., Ocon, S.S., Rock, R.S., and Spudich, J.A. (2002). Dynacortin Is a Novel Actin Bundling Protein That Localizes to Dynamic Actin Structures. *Journal of Biological Chemistry* *277*, 9088-9095.
50. Stock, A., Steinmetz, M.O., Janmey, P.A., Aebi, U., Gerisch, G., Kammerer, R.A., Weber, I., and Faix, J. (1999). Domain analysis of cortexillin I: actin-bundling, PIP2-binding and the rescue of cytokinesis. *EMBO J* *18*, 5274-5284.
51. Fang, X., Luo, J., Nishihama, R., Wloka, C., Dravis, C., Travaglia, M., Iwase, M., Vallen, E.A., and Bi, E. (2010). Biphasic targeting and cleavage furrow ingression directed by the tail of a myosin II. *The Journal of Cell Biology*.
52. Laporte, D., Coffman, V.C., Lee, I.-J., and Wu, J.-Q. (2011). Assembly and architecture of precursor nodes during fission yeast cytokinesis. *The Journal of Cell Biology* *192*, 1005-1021.
53. Fukata, M., Watanabe, T., Noritake, J., Nakagawa, M., Yamaga, M., Kuroda, S., Matsuura, Y., Iwamatsu, A., Perez, F., and Kaibuchi, K. (2002). Rac1 and Cdc42 Capture Microtubules through IQGAP1 and CLIP-170. *Cell* *109*, 873-885.
54. Faix, J., Clougherty, C., Konzok, A., Mintert, U., Murphy, J., Albrecht, R., Muhlbauer, B., and Kuhlmann, J. (1998). The IQGAP-related protein DGAP1 interacts with Rac and is involved in the modulation of the F-actin cytoskeleton and control of cell motility. *J Cell Sci* *111*, 3059-3071.
55. Bastounis, E., Meili, R., Álvarez-González, B., Francois, J., del Álamo, J.C., Firtel, R.A., and Lasheras, J.C. (2014). Both contractile axial and lateral traction force dynamics drive amoeboid cell motility. *The Journal of Cell Biology* *204*, 1045-1061.
56. Engler, A.J., Sen, S., Sweeney, H.L., and Discher, D.E. (2006). Matrix Elasticity Directs Stem Cell Lineage Specification. *Cell* *126*, 677-689.
57. Thomas, W.E., Vogel, V., and Sokurenko, E. (2008). Biophysics of Catch Bonds. *Annual Review of Biophysics* *37*, 399-416.
58. Ferrer, J.M., Lee, H., Chen, J., Pelz, B., Nakamura, F., Kamm, R.D., and Lang, M.J. (2008). Measuring molecular rupture forces between single actin filaments and actin-binding proteins. *Proceedings of the National Academy of Sciences*.
59. Robinson, D.N., Ocon, S.S., Rock, R.S., and Spudich, J.A. (2002). Dynacortin is a novel actin bundling protein that localizes to dynamic actin structures. *J. Biol. Chem.* *277*, 9088-9095.
60. Girard, K.D., Chaney, C., Delannoy, M., Kuo, S.C., and Robinson, D.N. (2004). Dynacortin contributes to cortical viscoelasticity and helps define the shape changes of cytokinesis. *EMBO J.* *23*, 1536-1546.
61. Faix, J., Steinmetz, M., Boves, H., Kammerer, R.A., Lottspeich, F., Mintert, U., Murphy, J., Stock, A., Aebi, U., and Gerisch, G. (1996). Cortexillins, major determinants of cell shape and size, are actin-bundling proteins with a parallel coiled-coil tail. *Cell* *86*, 631-642.

62. Weber, I., Gerisch, G., Heizer, C., Murphy, J., Badelt, K., Stock, A., Schwartz, J.-M., and Faix, J. (1999). Cytokinesis mediated through the recruitment of cortexillins into the cleavage furrow. *EMBO J.* *18*, 586-594.
63. Ren, Y., Effler, J.C., Norstrom, M., Luo, T., Firtel, R.A., Iglesias, P.A., Rock, R.S., and Robinson, D.N. (2009). Mechanosensing through cooperative interactions between myosin II and the actin crosslinker cortexillin I. *Curr. Biol.* *19*, 1421-1428.
64. Hu, C.-K., Coughlin, M., Field, C.M., and Mitchison, T.J. (2008). Cell polarization during monopolar cytokinesis. *The Journal of Cell Biology* *181*, 195-202.

CURRICULUM VITAE

VASUDHA SRIVASTAVA

Born in New Delhi, India on October 30, 1986

Johns Hopkins University
725 N. Wolfe Street, Physiology 100
Baltimore, MD 21205

E-mail: vsrivas4@gmail.com
Phone: (571) 606-3060

EDUCATION

- 2009-2015 Pre-doctoral Candidate in Chemical & Biomolecular Engineering
Johns Hopkins University, Baltimore, MD, USA
Expected graduation date: May 2015
- 2009 B.Tech/M.Tech in Biochemical Engineering & Biotechnology
Indian Institute of Technology Delhi, Hauz Khas, New Delhi, India

RESEARCH EXPERIENCE

- 2009-2015 *Pre-doctoral Research*
Molecular mechanisms of mechanosensing in *Dictyostelium discoideum*
Supervisor: Dr. Douglas N. Robinson, Professor, Department of Cell Biology, Johns Hopkins School of Medicine, Baltimore, MD, USA
- 2008-09 *M.Tech Thesis Project*
Identification of novel small non-coding RNAs (sRNAs) in *Bifidobacterium longum*
Supervisor: Dr. Jahar K. Deb, Professor, Department of Biochemical Engineering & Biotechnology, IIT Delhi, New Delhi, India
- 2008 *Summer Internship*
Rapid detection of bacteria using microarrays in microfluidic devices
Supervisor: Dr. Michel G. Bergeron, Director, Infectious Diseases Research Centre, Université Laval, Québec City, Canada
- 2006 *Summer Undergraduate Research Award (SURA), 2006*
Silver nanoparticle-lysozyme conjugates as Antimicrobial Agent/Protein Delivery Vehicle
Supervisor: Dr. Prashant Mishra, Associate Professor, Department of Biochemical Engineering & Biotechnology, IIT Delhi, New Delhi, India

RESEARCH ACTIVITIES

Research Publications

1. **Srivastava V.** and Robinson D.N. Mechanical stress and cytoskeletal network structure drive protein dynamics during cytokinesis. *Current Biology* 2015 (In Press)

2. Luo T., **Srivastava V.**, Ren Y. and Robinson D.N. Mimicking the mechanical properties of the cell cortex by the self-assembly of an actin cortex in vesicles. *Appl. Phys. Lett.* 2014; 104(15) 153701
3. **Srivastava V.** and Robinson D.N. 499. Cytokinesis. Lennarz & Lane eds. In *The Encyclopedia of Biological Chemistry*, Vol. 3, 2013; pp. 622-626. Waltham, MA: Academic Press
4. Kabacoff C., **Srivastava V.** and Robinson D.N. A summer academic research experience for disadvantaged youth. *CBE Life Sci. Educ.*, 2013; 12: 410-418
5. Sidhaye V.K., Chau E., **Srivastava V.**, Sirimalle S., Balabhadrapatruni C., Aggarwal N.R., Allesio F.R.D., Robinson D.N. and King L.S. A novel role for aquaporin-5 in enhancing microtubule organization and stability. *PLoS One*. 2012; 7(6): e38717
6. Luo T., Mohan K., **Srivastava V.**, Ren Y., Iglesias P.A. and Robinson D.N. Understanding the cooperative interactions between myosin II and actin crosslinkers mediated by actin filaments during mechanosensation. *Biophys. J.* 2012; 102(2): 238-247

Oral Presentations

- 2014 Frontiers of Cytokinesis Special Interest Subgroup, American Society of Cell Biology Meeting, Philadelphia, PA. “Dynamic interplay between cleavage furrow proteins in cellular mechanoresponsiveness”
- 2012 Center for Cell Dynamics, Johns Hopkins University School of Medicine, Baltimore, MD. “Cell topology changes and cell shape regulation”

Poster Presentations

- 2015 Biophysical Society Meeting, Baltimore, MD. “Dynamic interplay between cleavage furrow proteins in cellular mechanoresponsiveness”
- 2014 American Society of Cell Biology Meeting, Philadelphia, PA. “Dynamic interplay between cleavage furrow proteins in cellular mechanoresponsiveness”
- 2014 Biophysical Society Meeting, San Francisco, CA.
 a. “Mechanical stress-driven changes in the dynamics of cytoskeletal proteins”
 b. “Molecular Mechanisms of Contractility-based Cellular Mechanosensing”
- 2013 American Society of Cell Biology Meeting, New Orleans, LA. “Mechanical stress-driven changes in the dynamics of cytoskeletal proteins”
- 2013 US Human Proteomics Organization Annual Conference, Baltimore, MD. “The molecular basis for cellular contractility-based mechanosensing”
- 2013 Biophysical Society Meeting, Philadelphia, PA. “The molecular basis for cellular contractility-based mechanosensing”
- 2011 International *Dictyostelium* Conference, Baltimore, MD. “Changes in myosin II mechanosensory response using actin modulators”

EDUCATIONAL ACTIVITIES

Teaching

- 2010-14 Mathematics Curriculum Developer and Instructor, Summer Academic Research Experience (SARE), Johns Hopkins University School of Medicine, Baltimore, MD
- 2013-14 Science Curriculum Developer and Instructor, SARE Johns Hopkins University School of Medicine, Baltimore, MD
- 2010 Teaching Assistant, Chemical & Biomolecular Engineering Lab Johns Hopkins University, Baltimore, MD
- 2009 Teaching Assistant, Molecular Biology & Genetics IIT Delhi, New Delhi, India

Mentoring Activities

- 2014 John Hunyara, BCMB rotation student, Johns Hopkins School of Medicine
- 2013 Shantel Angstadt, Undergraduate, Elizabethtown College; INBT Research Experience for Undergraduates (REU), Johns Hopkins University
- 2013 Nathalie Gerassimov, BCMB rotation student, Johns Hopkins School of Medicine
- 2012 Dina Dajani, Undergraduate, University of Miami; Leadership Alliance, Summer Internship Program, Johns Hopkins School of Medicine
- 2011 Amanda Selsky, Student, Garrison Forrest High School; Johns Hopkins Women in Science and Engineering (WiSE) Program
- 2011 Samantha Miller, Undergraduate, Clemson University; Summer Intern
- 2010 Nurefsan Aksel, Undergraduate, Canakkale Onsekiz Mart University, Turkey; Visiting Summer Student

Educational Program Building

- 2010-14 *Founding Team Member and Instructor, Summer Academic Research Experience, Johns Hopkins School of Medicine*
The summer outreach program incorporates disadvantaged high school youth from Baltimore into research labs at JHU, while simultaneously providing them with remediation on basic skills in reading, writing, math, and science. I designed personalized math curriculum, delivered lessons, and evaluated student progress through regular assessments. I also helped develop an introductory science curriculum, and gave two lectures on molecular cloning. Further, I am a part of the team responsible for program and curriculum development, student selection, and progress evaluation.
- 2014 *Preparing Future Faculty Teaching Academy, Johns Hopkins University*
I am part of the first cohort for this program providing pedagogical training including overview of different education models, teaching and assessment skills, faculty mentorship, and hands-on teaching experience to doctoral students.
- 2014 *Institute for Excellence in Education Teaching Camp*
Johns Hopkins University School of Medicine, Baltimore, MD
- 2012 *Introduction to Effective Instruction Course*

ORGANIZATIONAL ACTIVITIES

Editorial Activities

- 2014 *Ad hoc* reviewer, PLoS One
2013-14 F1000 Associate Faculty Member
2012 *Ad hoc* reviewer, Biophysical Journal

Session Chair

- 2011 International *Dictyostelium* Conference, Session Chair, Baltimore, MD

Professional Societies

- 2013-Present American Heart Association
2013-Present US Human Proteomics Organization
2010-Present American Society for Cell Biology
2011-Present Biophysical Society

FELLOWSHIPS

- 2012-13 Isaac Morris Hay and Lucille Elizabeth Hay Graduate Fellowship,
Department of Cell Biology, JHU School of Medicine, Baltimore, MD
2008-09 Government of India Fellowship for Graduate Research
The Ministry of Human Resource & Development, Govt. of India

HONORS AND AWARDS

- 2014 ChemBE Graduate Research Award
Department of Chemical & Biomolecular Engineering, JHU, Baltimore
2013 Lewis Travel Award for ASCB 2013
Department of Cell Biology, JHU School of Medicine, Baltimore, MD
2006 Summer Undergraduate Research Award (SURA) 2006
Industrial Research & Development Unit, IIT Delhi
2004 Indian National Chemistry Olympiad (Selected amongst top 50 in India)
2002 National Talent Search Scholarship (Selected amongst top 1000 in India)
National Council for Educational Research and Training
2001 Junior Science Talent Search Scholarship (14th rank)
Directorate of Education, Delhi